VOLUME 45 2019 ISSUE 103

Helictite

Journal of Australasian Speleological Research

Published by Australian Speleological Federation
ISSN: 2652-483X (Online)

Helictite

Journal of Australasian Speleological Research
ISSN: 2652-483X (Online)

Helictite was established in 1962 by its foundation editors, Edward A. Lane and Aola M. Richards. It is intended to be wide ranging in scope from the scientific study of caves and their contents, to the history of caves and cave areas and the technical aspects of cave study and exploration. The territory covered is Australasia – Australia, New Zealand, the near Pacific Islands, Papua New Guinea and surrounding areas, Indonesia and Borneo.

In 1974 the Speleological Research Council agreed to support the Journal with financial assistance and in 1976 took over full responsibility for its production. From 1974 to 1997 the Journal was edited by Julia James assisted by other members of the Speleological Research Council Ltd. In 1998 Susan White and Ken Grimes took over as editors with Glenn Baddeley as Business Manager. Stefan Eberhard joined the editorial team in 2003.

In 2000 ownership was transferred to the Australian Speleological Federation, Inc. (ASF) and the Journal is administered by the Helictite Commission of the ASF.

Greg Middleton took over as Chief Editor in 2016. The accidental death of Ken Grimes in August 2016 led to further changes in editors, with Tim Moulds and Kevin Kiernan taking on the role.

The aim of the Helictite Commission of the Australian Speleological Federation is to publish the results of scientific studies in all fields of speleology in *Helictite – Journal of Australasian Speleological Research*.

Helictite in Digital Format

From 2017 Helictite is being published in digital format only. Papers are published online, and are freely available to all. There is no subscription fee – the ongoing costs of production and archiving are borne by the Australian Speleological Federation.

Submitted papers will still be reviewed and edited as before, but the layout may be varied to suit a digital format. Each paper will be published on line as it is ready as part of what is intended to be an annual volume. Intending authors should read the latest 'Information for Contributors' on the Helictite website.

Helictite web site

The Helictite web site is part of the parent ASF site. The URL is: http://helictite.caves.org.au

Helictite

Journal of Australasian Speleological Research

VOLUME 45 2019

Contents

Cover: The Overflow, Mammoth Cave, Jenolan. This only carries water during floods. During the 2017/18 drought it was dry – see paper by Murphy. Subject: Simon Murphy. Photo: Rafid Morshedi. Date: 14 Apr 2018.

Helictite, Volume 45, 2019 consists of a single issue.

All correspondence to: P.O. Box 269, Sandy Bay, Tasmania, Australia. E-mail: ozspeleo@iinet.net.au

This issue is published February 2020 (for 2019).

Explore, understand and protect

is the main goal of the

International Year of Caves and Karst

OBJECTIVES:

- improve public understanding of how caves and karst touch the daily lives of billions of people
- promote the importance of caves and karst through sustainable development, particularly in water quality and quantity, agriculture, geotourism/ecotourism, and natural/cultural heritage
- demonstrate how the study and proper management of caves and karst is critical to global economic and environmental health
- build worldwide educational capacity through activities targeted on cave and karst science
- promote awareness of the interdisciplinary nature of cave and karst science and management, and emphasize how interactions between different areas of science and management will be needed increasingly in future research, education and environmental protection
- establish durable partnerships to ensure that these activities, goals and achievements continue in the future beyond the International Year of Caves and Karst.

For more information, go to: http://iyck2021.org

Helictite, (2019) 45**:** 1-10

Gap Creek Valley and boulder caves within the Watagans National Park

Garry K. Smith[1]

[1]Newcastle and Hunter Valley Speleological Society Inc.
P.O. Box 15, Broadmeadow, N.S.W. 2292, Australia.

Abstract

The upper reaches of the Gap Creek valley are located in the Watagan Mountains, which form part of the Great Dividing Range to the west of Newcastle. The mountains in this vicinity are typically characterised by flat ridgelines, numerous sandstone cliffs, steep slopes and deeply fissured gullies. The steeply sloping valleys are eroded from sandstone and conglomerate bedrock. In many places 30 to 50 metre cliffs tower above, while other parts of the valleys have steep scree slopes covered in dense rain forest. Large boulders which have broken free of the cliffs over millennia, have tumbled down the slopes and lay scattered amongst the forest, with greater numbers found in the Gap Creek perennial tributary gullies.

A network of small caves have been created by the voids between the many boulders in the gullies and provide a habitat for a wide variety of fauna. Two of the larger caves have been surveyed and are described in detail. A literature search failed to locate any published material identifying the existence of boulder caves in the Gap Creek valley.

The protected valley contains three distinct forest types, which supports a wide variety of vegetation, including many tall tree species. Much of the valley's post colonial history is centred around the timber industry which thrived for more than a century in the area, before becoming part of the Watagans National Park.

Introduction

This paper discusses the geology, vegetation and history of the Gap Creek catchment within the Watagans National Park and details two boulder caves within this area. While the caves are relatively small compared to other know caves of this type around Australia, the Gap Creek caves are an important habitat for the variety of fauna which rely on the micro climate found within the caves beneath the rainforest canopy. This paper is the culmination of many years of exploration in the valley, searching for and documenting the caves and fauna they contain.

Geographic and geologic settings

The upper reaches of Gap Creek within the Watagans National Park, is 5 km north of Martinsville and 31 km West of Newcastle NSW, at an elevation >220 metres ASL. The valley can be accessed from Mount Faulk and Bangalow Roads, which enter the National Park from the South-East (Figure 1).

The Watagan Mountains make up a small portion of the Great Dividing Range, which stretches for more than 3,500 kilometres down the length of Australia's east coast. The exposed sandstone and conglomerate rocks, which make up the cliffs in the Watagan's Gap Creek area, were originally laid down as part of the Sydney Basin strata.

"Generally speaking the sedimentary history of the Sydney Basin is the result of a marine transgression at the end of the Late Palaeozoic glaciation, followed by a marine regression during the Late Permian and Triassic times. Major sedimentation ceased about the middle of the Triassic period" (Branagan and others 1976. p.2).

Subsequent tectonic events lifted the strata to form the Great Dividing Range about 50 million years ago. "More recently, volcanic flows covered large areas of the mountains in basalt. These have largely worn away, leaving only occasional outcrops on the high peaks" (Wikipedia 2018).

The Watagan Mountains consist of thickly bedded sandstone with lenses of conglomerate, dominated by the Hawkesbury and Narrabeen Group sandstones common within the Sydney Sedimentary Basin (Stone and others 2008). These Triassic sedimentary rocks formed between 208–245 million years ago (H-CRCMA 2009. p.4).

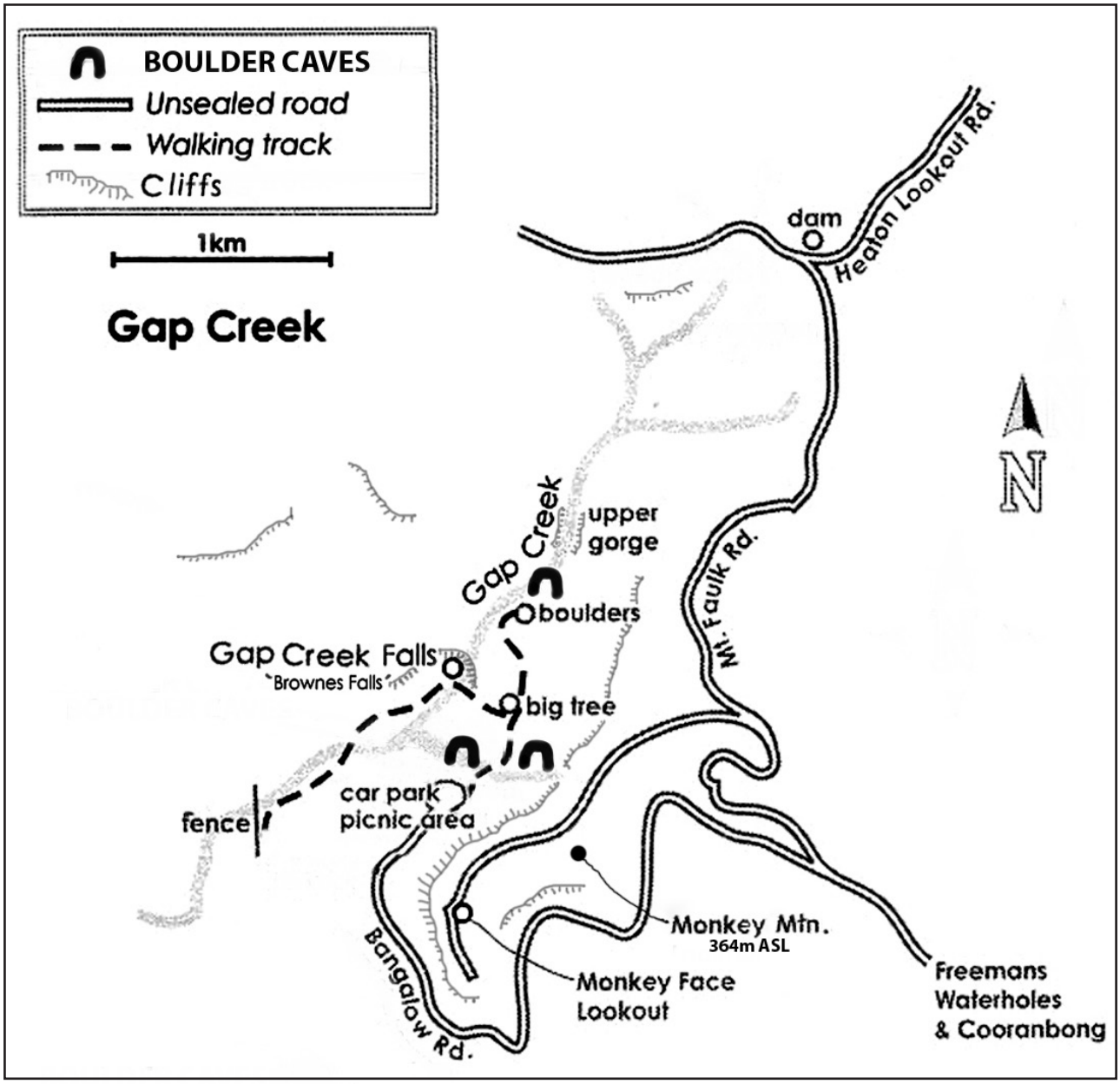

Figure 1. Location of caves within Gap Creek Valley.

Erosion over millions of years has created the present topography of the Watagan Mountains, which is characterised by flat ridgelines, numerous sandstone cliffs, steep slopes and deeply fissured gullies. The soils are generally acidic sandy loams with low to moderate fertility, and are highly erodible (Murphy 1993).

About 1 km to the south-west of the caves, is the National Park boundary and an abrupt end of the rainforest. A fence line marks the transition to private pastoral properties now cleared of the native vegetation.

The caves

Over millennia many large chunks of the conglomerate and sandstone cliffs have broken away and the boulders rolled down the slopes to collect in the gullies (Figure 2). The caves are created by these large boulders resting in the perennial stream gully near the end of Bangalow Road. The largest of these boulders is approximately the size of a double-decker bus. The voids between the boulders have formed a network of small caves (Figure 3).

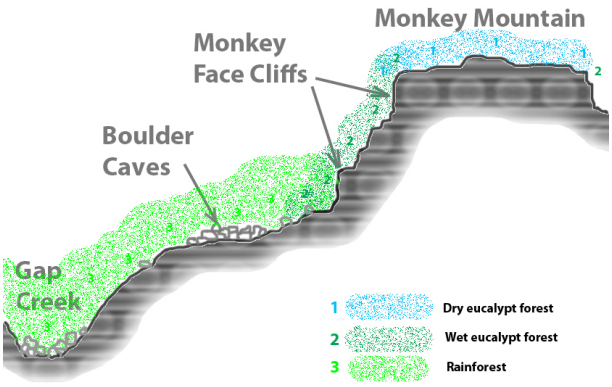

Figure 2. Section through Gap Creek and Monkey Mountain, showing location of caves and typical vegetation cover.

Figure 3. Cave created by boulders in a perennial creek bed. Photo G.K. Smith

Many of the boulders contain substantial eroded concave surfaces, which are consistent with the type of wind and moisture weathering caves occurring in nearby cliff faces (Figure 4). A number of the boulders containing significant weathered concave surfaces have come to rest with the concave surface facing down, so as to form a chamber beneath the boulder. There are examples in the two caves described as well as under stand-alone boulders scattered among the rainforest.

Figure 4. Cave under a large boulder which was originally a weathered cliff cave before breaking free of the escarpment and tumbling down into the gully. Photo G.K. Smith

The two largest known caves in the area are located in a tributary gully of Gap Creek near the end of Bangalow Road. They are the Bangalow Rock Pile Cave (I6E-68) (Figure 5) and the Log Jam Cave (I6E-69) (Figure 6). Both of these caves and several others located on Gap Creek above the falls, are at an elevation of ~260m ASL (Figure 1).

Several small streams flow beneath the boulders and through the caves. The streams are normally fed by seepage water from surrounding soils, however during periods of heavy rainfall, surface runoff from the cliffs above can turn the normal trickling stream into a fast moving flow. During extreme periods of drought, a number of small permanent pools in the caves, maintain a high humidity atmosphere within them all year round.

Bangalow Rock Pile Cave (I6E-68)

This cave is the most significant of the two caves described in this paper (Figure 7). There are four known entrances and a total survey length of 60m. It consists of several chambers connected by low crawl-ways along a perennial streambed. In many places throughout the cave, the boulders are resting on exposed bedrock, washed clean by turbulent water flow during times of flood (Figure 8).

Figure 7. Boulders in gully which have created part of Bangalow Rock Pile Cave (I6E-68). Photo G.K. Smith

Figure 8. Inside Bangalow Rock Pile Cave (I6E-68). Photo G.K. Smith

Several small chambers branch off the main passages at different levels. The upper levels are generally dry and frequented by bats while the lower levels are very damp and favoured by Glow-Worms.

Entrance No.4 is the most obvious entry point, however this is the most difficult entrance due to the 3.5m vertical drop and smooth boulder surfaces.

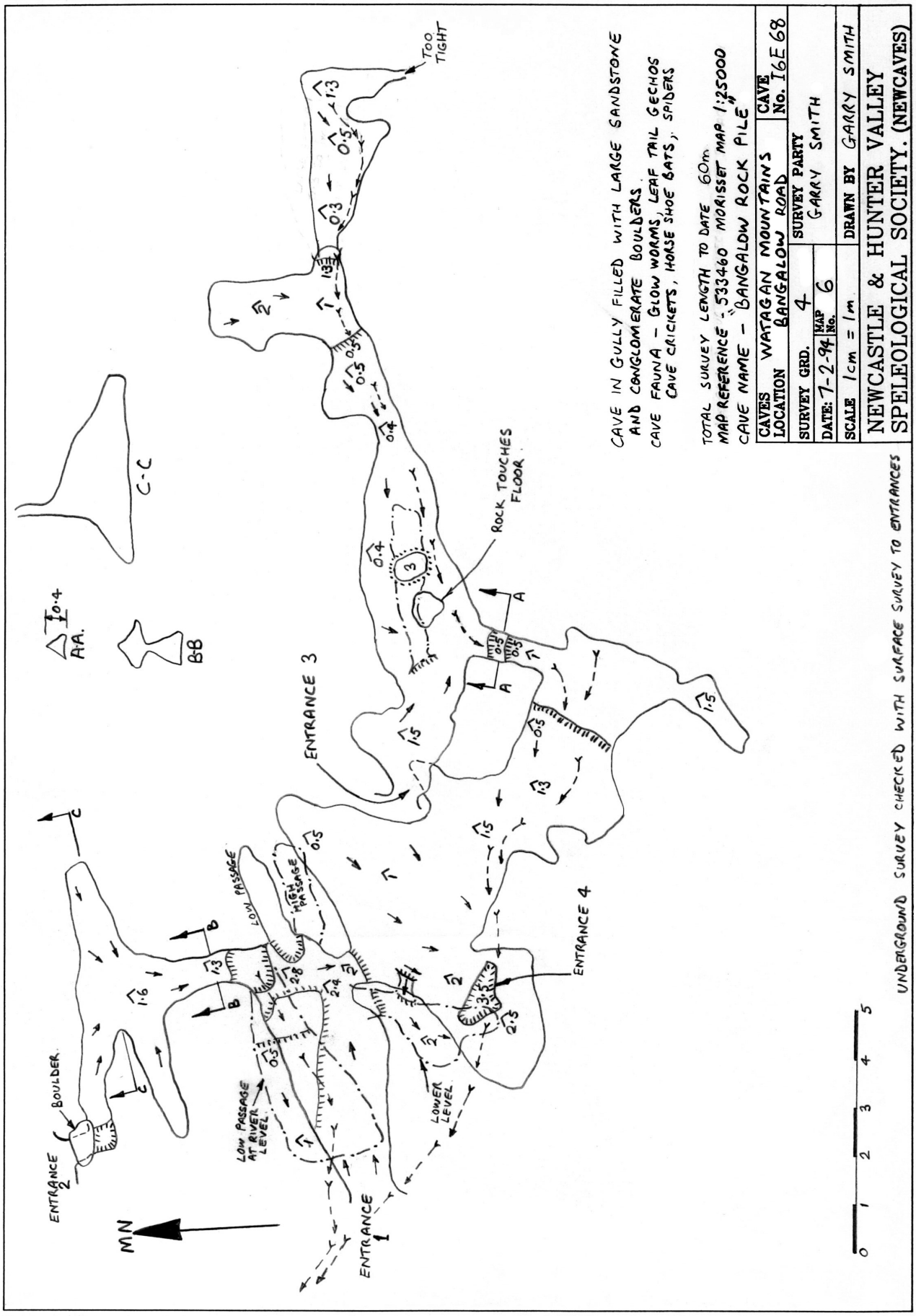

Figure 5. Bangalow Rock Pile Cave (I6E-68)

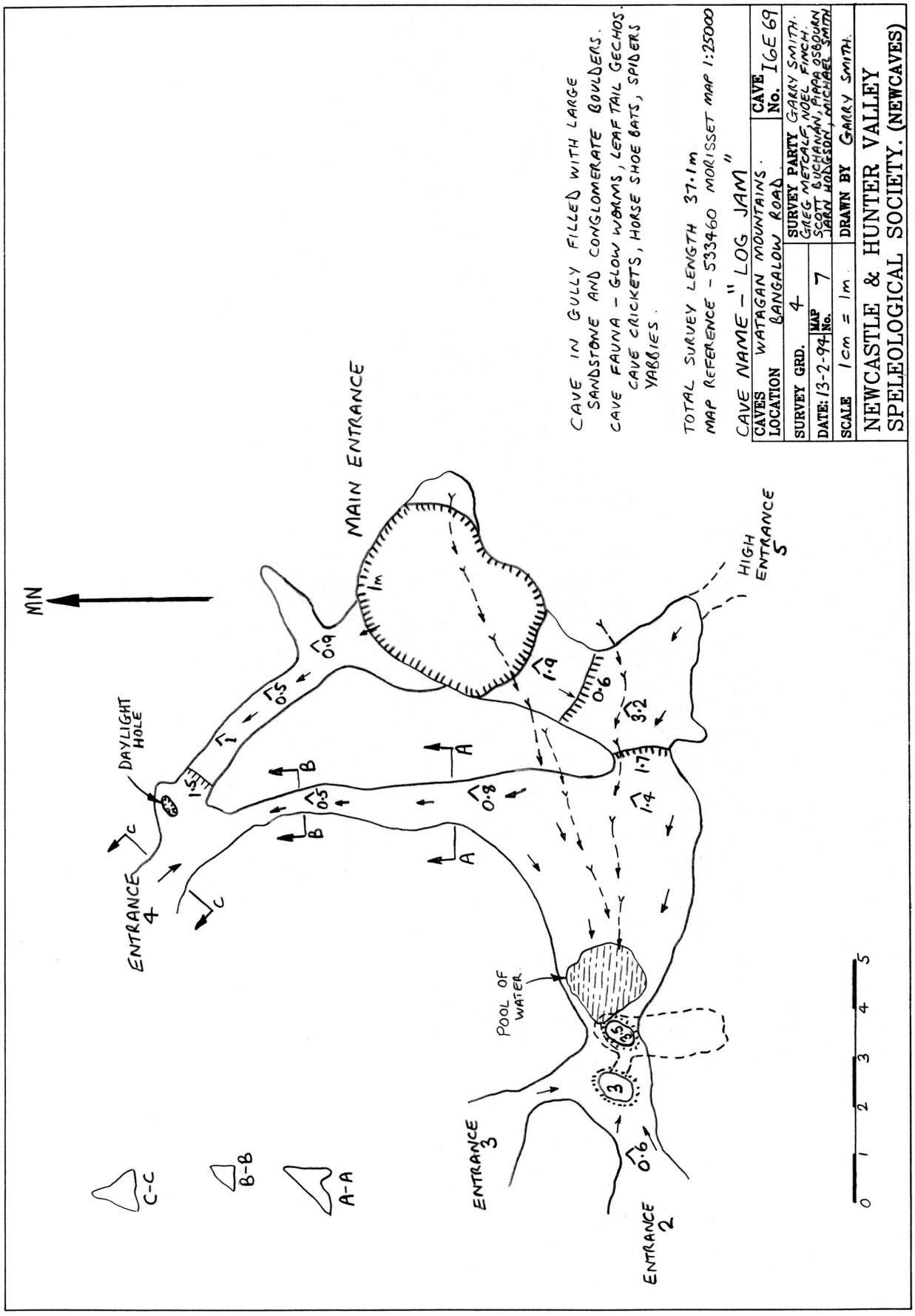

Figure 6. Log Jam Cave (I6E-69)

Gap Creek boulder caves

This entrance is directly above one of the larger chambers in the cave and allows some light to enter this chamber, however direct sunlight rarely penetrates the high forest canopy.

Log Jam Cave (I6E-69)

This cave has five known entrances and a total survey length of 37m. The main entrance is quite spacious and easy to access. There is a large section of exposed bedrock leading from the main entrance down to a pool, two metre diameter. From here several crawl-way passages with mud floors, can be followed to other entrances (Figure 9). After floods the crawl-ways may be full of forest debris, however this can easily be removed. Leaches have often been encountered near the cave entrances.

Figure 9. Cavers exiting via No.4 entrance of Log Jam Cave (I6E-69). Photo by G.K. Smith

No bats have been observed in this cave despite there being a couple of avens up to 3.5 metres in height.

Fauna in caves

Due to perennial streams and a number of permanent underground pools located in the cave's dark and twilight zones, a diverse range of water dependent fauna can be found below ground. These include: leeches, freshwater snails, fishing spider (*Dolomedes sp.*) freshwater shrimp, yabbies, tadpoles, diving beetles and mosquito larvae to name a few. The caves also supports a healthy population of glowworms *(Arachnocampa richardsae)*, Leaf-tailed Gecko *(Phyllurus platurus)*, millipedes, spiders, harvestmen, weta (*Australotettix montanus)*, Granny's Cloak Moth *(Speiredonia spectans)* and numerous other species of insects (Figures 10-14).

At various times of the year, up to 20 Eastern Horseshoe Bats *(Rhinolophus megaphyllus)* have been observed in the Bangalow Rock Pile Cave (Figure 15).

Above ground there are over 150 native animals and 130 species of birds recorded within Watagans National Park, some of which are listed as endangered or vulnerable species under the *Threatened Species Conservation Act 1995*. These include the following animals; brush-tailed rock wallaby, yellow-bellied glider, koala, spotted-tailed quoll and two bat species: the large-eared pied bat and the yellow-bellied sheathtail bat (NPWS 2010, pp. 15-16).

Leeches are very prevalent throughout the forest, particularly during and after wet weather. Ticks on the other hand are commonly found in the dryer parts of the forest, in particular where there is thick low-level vegetation.

Caves discovery and visitors

No written account of the caves or their discovery was uncovered during the research for this paper, however the author has personally known of the caves since the mid-1970s and their existence was known by a few Scouting leaders at the time. The caves have been explored by groups of Venturer Scouts as part of their Initiative Course between the late 1970s through to the late 1990s.

Since 2000, the caves have been visited on several occasions by members of the Newcastle and Hunter Valley Speleological Society Inc. (NHVSS) (Figures 16, 17, 18). However, the location of the caves is not widely known by the general public, thus the number of visitors is relatively low.

The general public frequently utilise the Gap Creek rainforest walking tracks within the Watagans National Park. The cliff faces below Monkey Face are frequently utilised by rock climbers and abseilers, as there are easy access tracks from top to bottom around the exposed rock faces. NPWS has also encouraged the general public to visit the forest, waterfalls and walking trails, by providing free campsites and well equipped picnic areas in the vicinity of the attractions.

Figure 10. Granny's Cloak Moth *(Speiredonia spectans)*

Figure 11. Glowworm *(Arachnocampa richardsae)*

Figure 12. Weta *(Australotettix montanus)*

Figure 13. Huntsman spider *(Heteropoda jugulans)*

Figure 14. Leaf-tailed Gecko *(Phyllurus platurus)*

Figure 15. Eastern Horseshoe Bat *(Rhinolophus megaphyllus)* >>

[All fauna photos above were taken in the Gap Creek boulder caves by G.K. Smith.]

Figure 16. Caver negotiates a squeeze in Bangalow Rock Pile Cave. Photo by G.K. Smith

Figure 17. Looking out the entrance of a boulder cave on Gap Creek. Photo by G.K. Smith

Figure 18. The author exploring a boulder cave at Gap Creek. Photo G.K. Smith

Flora of the valley

There is a wide variety of vegetation, ranging from rainforest in the gullies through to 'Moist Eucalypt Forests' and 'Dry Forests' on top of the ridges (Figure 2). The transition between the vegetation types can be very abrupt and occur due to cliff lines, valleys, soil composition and depth, and micro climate created by the topography. All three general vegetation types in the area, occur within a several hundred metre radius of the caves.

The vegetation at Gap Creek can be categorised into three broad forest types. However as there are a vast number of plant species which comprise the forest types, it would be impractical to include a complete list in this paper.

Rainforest

Smaller areas of warm-temperate sub-tropical rainforest and paperbark palm forests occur in sheltered gullies and creek-lines (Figures 19 & 20). Typical rainforest species include lilly pilly (*Acmena smithii),* sassafras (*Doryphora sassafras*), brush cherry (*Syzygium australe*), wild quince (*Guioa semiglauca*), coachwood (*Ceratopetalum apetalum*) with tree ferns (*Cyathea australis, C. leichhardtiana, C. cooperi*), climbing vines and epiphytes common beneath the canopy. Isolated stands of red cedar (*Toona ciliata*) and Illawarra flame trees (*Brachychiton acerifolius*)

Figure 19. Rainforest vegetation in Gap Creek.
Photo by G.K. Smith

Figure 20. Strangler Fig and vines growing over a boulder in the Gap Creek rainforest.
Photo by G.K. Smith

remain in more remote areas (NPWS 2010, pp.11-12).

The paperbark palm forests contain a number of melaleuca species (*Melaleuca biconvexa* and *M. linariifolias*) with white bottlebrush *callistemon salignus*) and cabbage tree palms (*Livistona australis*) (NPWS 2010, pp. 11-12).

Moist eucalypt forests

Watagans National Park and adjacent Jilliby State Conservation Area contain similar vegetation types. Tall moist eucalypt forests are widespread in the reserves and predominately occur on the higher slopes below the ridge line down to the fringes of the rainforest. They commonly contain turpentine (*Syncarpia glomulifera*), mountain blue gum (*Eucalyptus deanei),* white mahogany (*E. acmenoides*), Sydney blue gum (*E. saligna*), blue-leaved stringybark (*E. agglomerata*), blackbutt (*E. pilularis*) and grey gum (*E. propinqua*) with warm temperate rainforest influences dominating the understorey of these communities (NPWS 2010, pp. 11-12).

Dry forests

This forest type is found predominately on the ridge top where soil depth is shallow. Forest oak (*Allocasuarina torulosa*), Sydney peppermint (*E. piperita*), broad-leaved white mahogany (*E. umbra*), large fruited red mahogany (*E. scias subsp. scias*), smooth-barked apple (*Angophora costata*) and red bloodwood (*Corymbia gummifera*) are common in the drier forest areas with understoreys varying from open dry and grassy, to dense shrubbery (NPWS 2010. pp.11-12).

Land surrounding the National Park is used predominantly for forestry, with grazing and smaller

rural residential hobby farm lots in the foothills and valleys below (NPWS 2010. p.1).

History of the area

The original inhabitants of the Watagan Mountains are the Awabakal and Darkinjung Aboriginal peoples. Evidence of their occupation can be found throughout the area in the form of occupation and art sites, engravings and axe grinding grooves (NPWS 2010 pp. 18-19). Watagan is an Aboriginal word meaning "many ridges" (Ray 1993).

European use of the area began in the early 1820s, with the arrival of the cedar getters. Hardwood harvesting followed, bolstered by demand during the construction of the nearby Newcastle - Maitland rail link in the 1850s. A timber supply route to the coast via Dora Creek helped to keep up with the timber needs of the growing coal mining industries. During the 1970s and 1980s, local saw-millers received substantial contracts to supply sleepers for the construction of the rail line between Newcastle and Sydney (NPWS 2010, p.21-22).

Timber was the backbone of the local economy and four large steam-driven timber mills were operating in the area in the 1870s (Anon. 2009). Cedar trees grew in abundance throughout the Watagan Mountains and it was a very sort after timber for furniture. The early (colonial cedar) trade saw most of the cedar shipped off to England to supply an insatiable market for fine softwoods. (NPWS, 2010. pp. 21-22).

The early roads in the mountains were developed from the original bullock tracks used to extract logs. Timber production from the mountains was increased through the construction of tramways, loading points and elaborate mechanical flying foxes to lift or drag logs to the sawmills (NPWS 2010).

The demand for railway sleepers generated by the construction of the Sydney-Newcastle railway caused a boom up till its completion in the late 1880's.

In 1916 the creation of the Forestry Commission (now Forests NSW) saw much of the Watagan Mountains set aside as State Forest (NPWS 2010). By 1936 the Forestry Dept had resumed all the land and declared the whole of the Watagan Mountains as a forest reserve for the growth of timber (NPWS 2010, p. 22).

At this time, the newly created Olney State Forest encompassed 44,000 hectares and included the area where the caves are located. Large plantations of Blue-leafed Stringy Bark and Blackbutt were planted in parts of the forest during the 1960s and 70s, to supplement selected timbers (NPWS 2010).

During World War II the forests were almost entirely stripped of their softwoods, particularly coachwood, which was used for the Diggers' .303 rifle and for the construction of the Mosquito fighter plane (Anon. 2009).

Monkey Mountain and Monkey Face lookout, which overlooks the Gap Creek valley containing the caves is named after Monkey, an old lead bullock from the timber-getting days. Monkey was owned by the Browne family, who were among the early settlers, timber-getters and sawmillers in the area. There are two stories circulating about Monkey. One was that Monkey liked to hide, in its spare time, on a mountain shelf below the top of the cliff line (Anon. 2009) and the other is that it led the whole bullock team over the cliff to their death (Powell 2003). Hence the names Monkey Mountain and Monkey Face (Figure 1).

The 40 metre high Gap Creek Falls has only been known by that name since about the mid-1990s (Figure 1). Historically they were known as Brownes Falls - named after the aforesaid pioneering saw milling family in the Martinsville valley. After rain the water topples in wide sheets and veiled cascades over the falls into the broad plunge pool below. The grotto at the base of the falls is very similar to many found in the Blue Mountains.

The Watagans National Park, covering an area of 7,798 hectares, was created through the enactment of the *Forestry and National Park Estate Act 1998* on 1 January 1999, under which parts of three state forests were combined and transferred to the National Parks and Wildlife Service (NPWS 2010, p. 1). This included the Gap Creek Valley previously under the control of the NSW Forestry.

Another 47 hectares was added to the National Park in 2007 (NPWS 2010).

A draft plan of management for Watagans National Park was placed on public exhibition from 5 December 2008 to 30 March 2009. The final management plan was adopted by the Minister for Climate Change and the Environment on 10 December 2010.

Weather

The official Bureau of Meteorology records show that the Olney State Forest has a yearly temperature range between 0°C and 37°C. However, the average temperature range is between 16°C and 30°C in summer and between 5°C and 16°C in winter. The area's highest recorded rainfall is 91.4mm during one day and the average annual rainfall is approximately 1.5 m.

Due to the abrupt transition in elevation from the Eastern coastal lowlands at < 100 m, the Watagan Mountain ridges at > 400 m receive a higher than average rainfall. Nestled between the mountains, the Gap Creek valley, also receives a high average rainfall as well as the runoff from the surrounding ridges. In addition, the high mountain ridges protect the valley from severe winds, which makes it ideal for growth of high canopy rainforest vegetation. These conditions have created a relatively moist micro-climate beneath the rainforest canopy and within the caves.

Acknowledgements

Thank you to the NSW Department of Environment & Climate Change and National Parks & Wildlife Service, for the use of information in their plan of management.

I would like to especially thank Jodie Rutledge for her helpful suggestions regarding this paper.

References

Anon. 2009 'Traveller Cooranbong.' http://www.traveller.com.au/cooranbong-5ypu Accessed 28 May 2018. Published 1 January 2009.

Branagan, D., Herbert, C. and Langford-Smith T. 1976 *An outline of the geology and geomorphology of the Sydney Basin*. Science Press for Department of Geology and Geophysics, University of Sydney, Sydney.

H-CRCMA 2009 *Where land meets water-resource kit: Central Coast supplement: A guide to riparian management in the Hunter Valley*. Hunter-Central Rivers Catchment Management Authority, Paterson. 20 pp.

Murphy, C.L. 1993 *Soil landscapes of the Gosford-Lake Macquarie 1:100,000 sheet report*. NSW Department of Conservation and Land Management, Sydney.

NPWS 2010 [National Parks and Wildlife Service, NSW, part of Department of Environment, Climate Change and Water] *Watagans National Park and Jilliby State Conservation Area: plan of management.* http://www.environment.nsw.gov.au/resources/planmanagement/final/20101032WatagansJillibyFinal.pdf Accessed 28 May 2018.

Powell, G. 2003 *Hunter Valley bushwalks*. Kingsclear Books, PO. Box 335 Alexandria. p. 56.

Ray, Greg 1993 The Aboriginal hunter. Supp. to *The Newcastle Herald,* 11 May 1993. 4 pp.

Stone, C., Kathuria, A., Carney, C. and Hunter, J. 2008 Forest canopy health and stand structure associated with bell miners *(Manorina melanophrys)* on the central coast of New South Wales. *Australian Forestry,* 71(4): 294-302. http://svc043.wic023v.server-web.com/pdf/pdf-members/afj/AFJ%202008%20v71/4/07Stone.pdf Accessed 28 May 2018.

Wikipedia (The Free Encyclopedia) 2018 'The Blue Mountains and Great Dividing Range' http://en.wikipedia.org/wiki/Blue_Mountains_National_Park Accessed 28 May 2018

Helictite, (2019) 45**:** 11-26

On the 2017/2018 drought at Jenolan Caves

Simon J. Murphy[1, 2]

[1] School of Physics, University of Sydney, NSW 2006, Australia.
[2] Sydney University Speleological Society, PO Box 3318, Redfern NSW 2016, Australia.
simon.murphy@sydney.edu.au

Abstract

A severe drought is currently (September 2018) affecting Jenolan Caves, NSW, both above and below ground. Rainfall data are analysed to show that this drought has surpassed the once-in-25 years level and is now a once-in-a-century event. This is the second-driest period since records began in 1895, and the driest in 115 years. The water levels observed in rivers, pools and sumps of selected caves are documented, revealing the driest subterranean conditions observed there to date. Underground river flow rates are at record lows. A warming climate is enhancing the severity of the present drought, compared to historical events of similarly low rainfall.

1 Introduction

The Jenolan Caves Limestone dates to the mid-Silurian (~430 Ma) and exists as a narrow belt that runs predominantly NNW-SSE with a perpendicular width ranging from 50 to 350 m (Branagan and others 2014). The geology has been described by Shannon (1976), with updates from Cooper (1990, 1998) and Branagan and others (2014). A map is provided in Figure 1. The road to Jenolan Caves cuts through the limestone at the natural Grand Arch, dividing the limestone into a southern area of 2.3 km and a northern area that outcrops nearly continuously for 4 km with isolated outcrops for a further 3 km. It is the Northern Limestone that contains the largest caves and has a much larger water catchment, hence is the focus of this paper.

To the north of the Grand Arch, the Jenolan River has carved a gorge into the limestone. This gorge transitions to alluvial flats around 1 km north up the valley at Playing Fields. The Jenolan River only flows during flood, but its dry bed can be followed north through gorges and across alluvial flats for up to 5 km, depending on recent rainfall, beyond which the river is on slate and always flowing. The Jenolan River and various minor tributaries divide the limestone into several bluffs.

Throughout the valley the limestone dips to the west, sometimes near-vertically, and is overturned in places. The full depth of the limestone is unknown, though dry sections of Mammoth Cave can be found 180 m below the surface. Slug Lake in Mammoth starts 65 m below ground, has been dived 96 m, and continues deeper out of sight (Vaughan-Taylor & Ryan 2000). Clearly, the near-vertical bedding allows large quantities of water to penetrate deep underground.

A hydrological model for Jenolan Caves was proposed by Shannon (1976) and Dunkley (1976). It includes three principal components: (i) the surface flow, derived mostly from the Jenolan River as it flows off the slate and into the U-shaped valley, supplemented by minor tributaries entering the valley from the east and west; (ii) the subsurface reservoir, consisting of alluvial storage located towards the northern end of the valley, being approximately 15 ha in area and ranging from 15 to 40 m in depth (Kelly 1988). This aquifer is usually assumed to have 20% porosity (Cooper & Staraj 1996) and it follows that its capacity is around 2.5 Gl (Cooper 2010); and (iii) the Jenolan Underground River (JUR) and underwater lakes that exist in voids in the limestone, some of which have been observed in drought for this work.

There are many stream sinks on the surface conducting water down to the subsurface, but with limited capacity (Figure 2). Hence under heavy rain conditions, or when the subsurface reservoir is full, the surface stream advances down the valley. In heavy flood, the surface stream flows all the way to the Grand Arch; in drought the low stream flow sinks into the alluvium as it leaves the slate. The latter describes the conditions observed at Jenolan Caves during this work (Apr – Aug 2018).

The exact path and location of the JUR are unknown north of Mammoth Cave. Given the dip of the limestone, it is expected that the river is located further west with depth beneath the surface, as seen clearly in the development of cave passage in Mammoth. It may therefore be expected that the

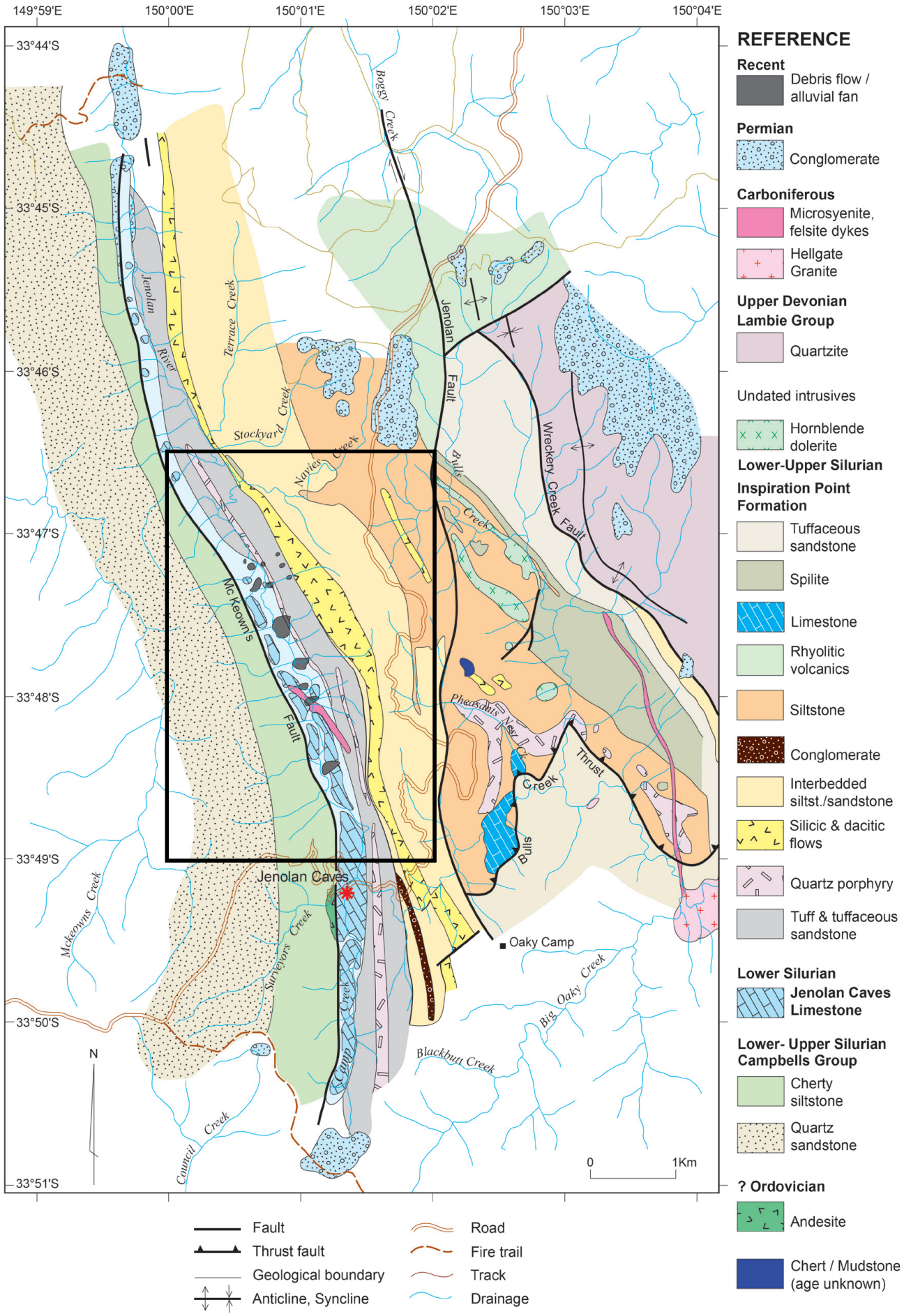

Figure 1. Geology of the Jenolan Valley, according to Branagan and others (2014). The unlabelled layer in the valley floor between the Jenolan Caves limestone bluffs is also debris flows / alluvial fans. The black outline shows the region that is annotated in Figure 2. *Reproduction by permission of author and journal.*

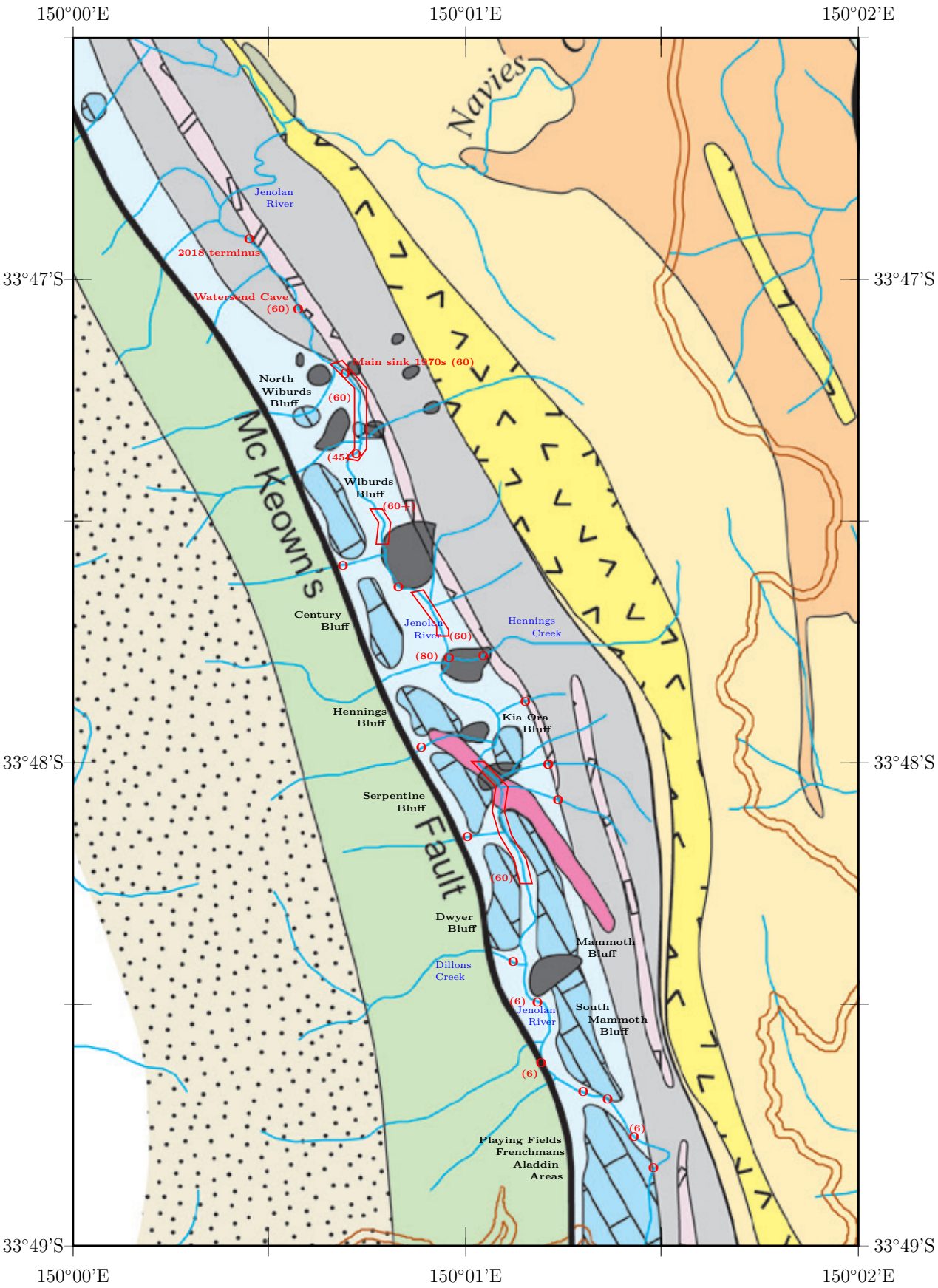

Figure 2. The Northern Limestone, enlarged from the map in Figure 1. See there for key. Stream sinks and their capacities from Shannon (1976) are highlighted in red, with several new additions, particularly sinks in side creeks from Cooper (pers. comm.). Sink positions are true with respect to the river, but some surface geology is in need of updating (Cooper, in prep.).

JUR lies under the limestone on the western side of the valley (Staraj & Cooper 1996). The JUR is first observed in the southern section of Mammoth Cave, where it is known as Lower River. It emerges from a hole in the western wall, is exposed for less than 20 m, then disappears again into a hole in the eastern wall. It later joins Slug Lake approximately 6 m below the lake's surface (or less in drought, when the water level is lower). It is audible or visible near the Lower River area of Mammoth Cave through slots or connected bodies of water such as Grinning Monster Lake. It was dived upstream to −50 m by Rod Obrien before becoming too dangerous to dive further (described by Johnston 2014). After becoming lost in Slug Lake, the JUR is next seen in Spider Cave, another kilometre downstream. Its path between Mammoth and Spider caves is unknown. However, once picked up at End Zone, at the northern end of Spider Cave, its path can be followed or dived south all the way through the show caves to the Blue Lake.

The subsurface reservoir appears capable of supplying water to the JUR even in extended droughts such as the present one. Cooper (2010) argued that the reservoir can supply 60 l/s for ~450 days. Lower River has never been observed to stop flowing, though its flow rate does change from around 60 l/s in drought to well over 500 l/s in flood,[1] with a normal flow rate of around 140 l/s.

Drought and flood each offer conditions that can further our understanding of karst landscapes. Hydrology based on flood events can shed light on potential connections between caves and thereby suggest opportunities for exploration and linking caves. At the same time, as flood waters recede, stream sinks become more obvious and their capacities can be measured. On the other hand, floods create sumps and can exclude large sections of cave from exploration for some time. During drought, sumps can dry out and allow for rare access.

Cooper (2010) noted that the northern catchment at Jenolan Caves is 25 km^2; the southern catchment is 2.7 km^2. Given that each mm of rain contributes 1 Ml of water per km^2, then a modest rainfall of 4 mm dumps 100 Ml into the northern catchment. Hence, downpours can bring volumes of the order of 1 Gl. While this is the approximate capacity of the alluvial reservoir, much of this water will be absorbed in topsoil before it can be channeled into the valley floor. Nonetheless, floods can occur very rapidly indeed when the alluvium is already charged. Droughts, on the other hand, develop on timescales of around a year.

In this article, rainfall data are analysed for evidence of a severe drought, accompanied by observations of changing conditions underground. While this drought has been developing since April 2017, it only came to media attention around April 2018. In the greater Sydney area, some major reservoirs such as the Cataract and Cordeaux dams are down on capacity by more than 50% compared with the same time last year. The largest of these reservoirs, the Warragamba Dam, lost 22% of its volume, corresponding to 450,000 Ml of water. State-wide the drought is having a devastating impact on farming. In Sect. 2 the rainfall data and processing of those data are described. Sect. 3 shows how these rainfall data indicate a severe and ongoing drought. In Sect. 4 it is shown that the climate has been warming over the past half-century and it is argued that this intensifies the drought. Sect. 5 documents observations of water levels and flow rates at Jenolan Caves.

2 Rainfall observations

Rainfall data for Jenolan Caves (station number #063036) were downloaded from the Australian Bureau of Meteorology website.[2] Rainfall data were first collected for Jenolan Caves on 1 Apr 1895, and were taken daily almost uninterrupted until Mar 1976, when a hiatus of 10.8 yr began. Since the resumption of observations on 1 Jan 1987, there have been only minor interruptions to data collection (Figure 3).

In this paper the primary interest is in relative differences in rainfall as indicators of drought. While the absolute rainfall amounts are unquestionably important, there is some concern about the suitability of the Jenolan Caves station for this purpose, due to its location near a wall that would likely cause the rainfall to be underestimated. However, comparison with two nearby stations partially allays this concern. Little Hartley, 17.3 km to the north-east, and Oberon Springbank[3], 23.9 km to the north-west, each have annual mean rainfall totals *lower* than Jenolan Caves, at 777.0 and 837.2 mm, respectively, compared to Jenolan Caves' 961.4 mm. The higher rainfall at Jenolan Caves is likely because the station, at 792 m, is

1: It is not possible to observe the maximum flow rate of Lower River in flood, because this area becomes inaccessible.

2: http://www.bom.gov.au/jsp/ncc/cdio/weatherData/av?p_nccObsCode=136&p_ display_type=dailyDataFile&p_startYear=&p_c=&p_stn_num=063036

3: This station appears to have changed name to Oberon Albion St. in 2018.

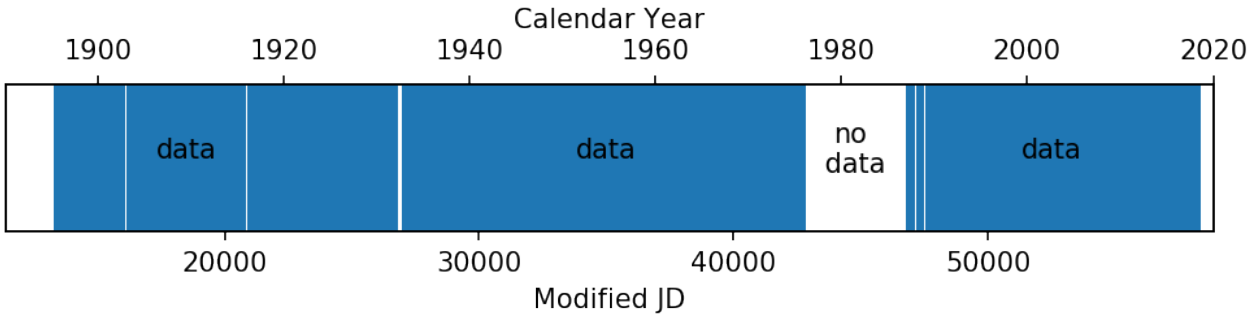

Figure 3. Coverage of rainfall data at Jenolan Caves, station #063036. Blue-shaded regions denote dates with rainfall coverage, while white regions have no data. The most recent blue shading extends to the time of writing (15 Sep 2018). The bottom axis is modified Julian date, defined as JD−2 400 000.5.

Table 1. Weather station data. The penultimate column gives linear distance from Jenolan Caves and the final column gives the mean annual rainfall. The Katoomba station is not used for rainfall analysis, but is used for temperature analysis in Sect. 4.

Name	Number	Lat. deg.	Long. deg.	Altitude m	Opened	Dist. km	Mean mm
Jenolan Caves	063036	−33.82	150.02	1792	1895	10.0	961.4
Little Hartley	063072	−33.70	150.13	1655	1951	17.3	777.0
Oberon Springbank	063063	−33.67	149.83	1053	1888	23.9	837.2
Katoomba Murri St	063039	−33.71	150.31	1015	1895	29.1	(1401.9)

surrounded on all sides by hills over 1100 m within a few kilometres. Details on the stations are given in Table 1. The large and unpopulated Kanangra-Boyd National Park lies to the south and east of Jenolan Caves, leading to a paucity of nearby weather stations in those directions.

Rainfall values are occasionally provided as accumulated totals, sometimes spanning a few days. Days within the accumulated interval are left with no data, giving the appearance of a gap in the data. On these days within the accumulated interval, the amount that fell is set to zero, thus treating the data as if all the rain over the interval fell in the final day. The interval is never greater than five days; only once in the entire record for Jenolan Caves is the interval five days, and only five times is the interval four days.

The nearby stations at Little Hartley and Oberon Springbank serve another useful purpose in filling gaps in data collection at Jenolan Caves. One of the summary statistics considered here is the cumulative rainfall over one-year periods (but not necessarily calendar years), which is unreliably computed when there are gaps in the data. For single-day gaps that are not due to accumulation of rainfall totals, such as 10 Sep 2016, and the occasional month-long gap such as Dec 1988, the use of data from nearby stations is useful and acceptable. Care is taken in quoting results from the 10.8-yr gap between 1976 and 1987, and throughout this article note is made of where this has been done.

To illustrate the validity of importing observations from nearby stations in this way, the correlation between rainfall totals is shown in Figure 4. The Spearman's Rank correlation coefficients between each station and Jenolan Caves are both 0.66. Outliers are likely due to thunderstorms affecting one station only.

When importing data from the two nearby stations, corrections are made for the difference in annual rainfall at these locations. The correction factor is the ratio of annual rainfall at the relevant locations. Thus when calculating the missing Jenolan Caves rainfall from the Oberon Springbank rainfall, the values are multiplied by (961.4/837.2 =) 1.148. Similarly, the factor for Little Hartley is 1.237. If both Little Hartley and Oberon Springbank have data available, the mean of their corrected values is used.

Note that Figure 4 suggests that rainfall at Jenolan Caves tends to be quite localised. This is consistent with field reports. In his article *Jenolan: Where it never rains but it floods!*, Staraj (1989) noted that on a seemingly dry Jenolan weekend[4], where it hadn't rained in Sydney for a few days prior, the surface creek was flowing in its usually dry bed and sinking as far south as Spider Cave.

4: The trip dates were 1–2 July 1989. Rainfall over the 5 days prior was [0.0, 0.8, 1.4, 1.6, 0.0] mm. While this is probably insufficient to cause the surface creek to flow, the week before that saw 53.6 mm, which is three quarters of the median June rainfall.

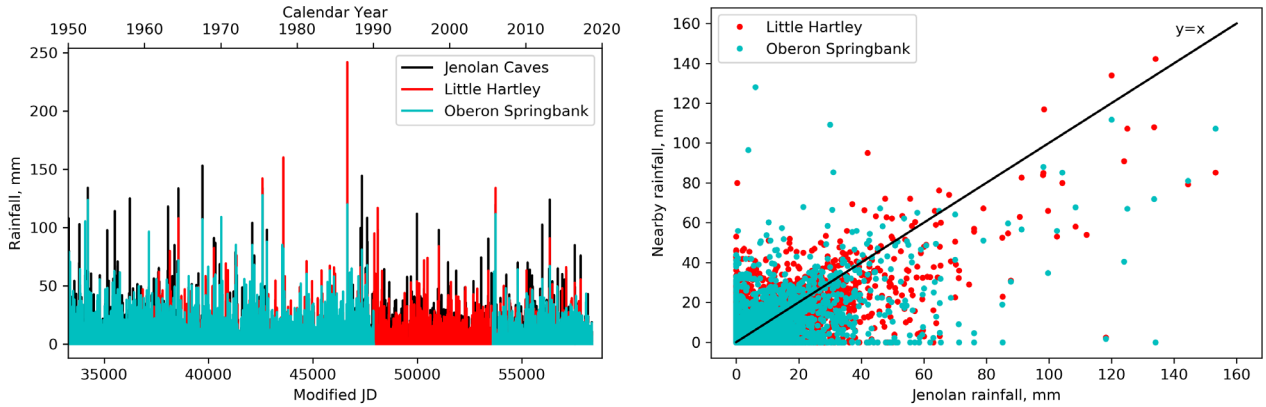

Figure 4. *Left:* Rainfall at the three sites since 1950, indicating correlation between sites at least for the larger rainfall events, though Jenolan Caves generally receives more rain in such events. For better visibility, lines have thicknesses greater than one day, giving the false impression that the rainfall never reaches zero. *Right:* The *y* axis shows how much rain fell at nearby sites on occasions where *x* mm fell at Jenolan Caves. Data are shown for each day on which data overlap between Jenolan Caves and another station. The diagonal line is not a fit to the data, it is the line *y*=*x* to guide the eye. This panel also shows that Jenolan Caves receives more rain than nearby sites.

3 Evidence for drought in rainfall data

Comparison of rainfall totals year-by-year reveals that 2017 was the driest year of the decade so far, and 2018 is the driest start to a year this decade as well. In fact, at no time in the past 30 years has a year started with anywhere near as little rainfall as 2018 has to-date (analysis fixed at 15 Sep 2018). Comparisons for the past 30 years are shown in Figure 5. Note that 1965, 1940 and 1902 are the only three years to have started drier (to 15 Sep) than 2018 (not shown in the figure, and excluding the hiatus years). Only 346 mm fell to 15 Sep in 2018.

The end of 2017 was dry and the start of 2018 was dry, hence the total rainfall over the 365-day interval ("1-year cumulative rainfall") was extremely low – much lower than any time in the previous 30 years (Figure 6). This way of analysing rainfall data makes droughts much clearer in the data, and better highlights their duration and severity. It is also more meaningful than plotting calendar years, since the levels of lakes and flow rates of rivers are insensitive to our choice of calendar.

The same data also reveal changes in rainfall on time-scales of decades. The period c.1895–1940 was generally dry, with a particularly dry period in the late-1930s to 1940. From the mid-1940s to the mid-1950s rainfall increased dramatically and was quite erratic from one year to the next. Then a generally wet period followed, lasting until the late 1970s, which included the largest flood to affect the Northern Catchment on record, in 1975 (Welch 1975). For the period around 1980 caution must be exercised because data are only available by importing from nearby weather stations, but the late-1970s and early-1980s were dry, consistent with field reports. The late 1980s and 1990 were particularly wet years, with 1990 being the last year in which a lake was observed in Wiburds Lake Cave (Cooper 2010). Since the early-1990s, Jenolan Caves has been relatively dry, except for a blip in 2010. This might be identified as the "Millennium Drought" which stretched from the mid-1990s until the terminating La Niña in 2010-2011. However, after the La Niña, the rainfall appears to have returned to "Millennium Drought" levels that are comparable to rainfall before the 1950s. The data do not go far back enough in time to establish a particular periodicity to this variability, nor to assess whether anthropogenic effects are at play.

It is difficult to compare the relative rarity of floods and droughts, partly because the timescales involved are different: droughts take time to develop but last a long time, whereas floods are more frequent but shorter lived. One can make comparisons against over-simplified scenarios, though, to see how rare extreme-weather events of each type are.

A downpour of 50 mm supplies around 1.25 Gl of water to the northern catchment, which is half of the reservoir volume. Thus, if the reservoir is more than half full, there will be a flood. Of course, if the reservoir is already full, much smaller amounts can cause flood, but the reservoir might also be less than partially filled when the hypothetical 50-mm downpour occurs, so let us take that as a first estimate. That gives us 177 such events in the rainfall record since records began in 1895. That seems approximately correct for this location: around two flood events occur per year, even if

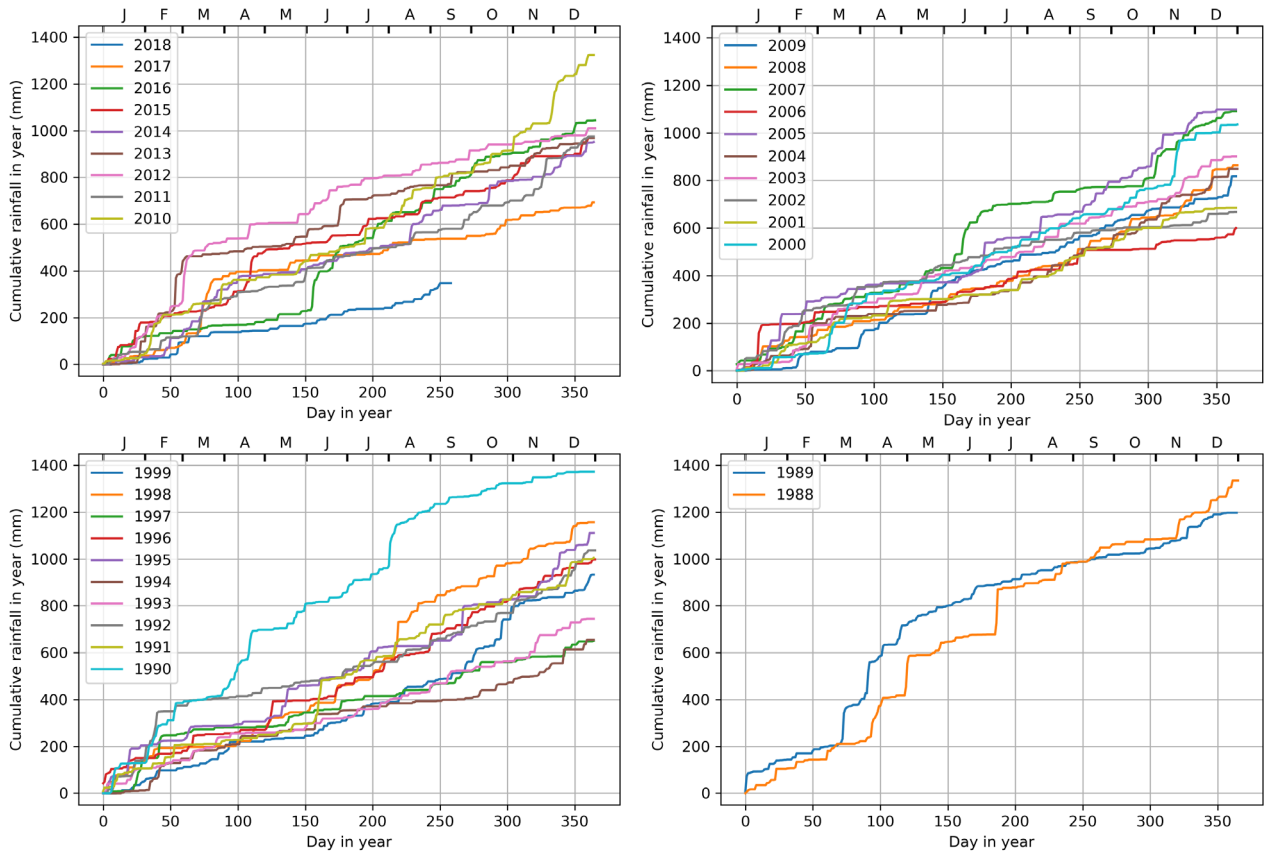

Figure 5. Year-by-year cumulative rainfall comparisons for the past 30 years, separated by decade. Rainfall data for the Jenolan Caves station are unavailable for the rest of the 1980s (Sect. 2). The mean annual rainfall at this location is 961 mm. Panels all have the same vertical scale.

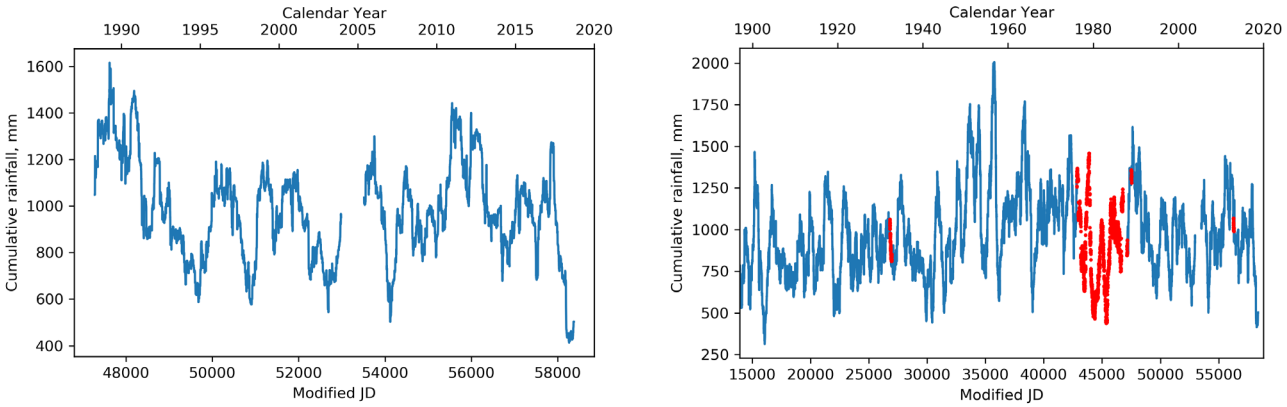

Figure 6. *Left:* 1-year cumulative rainfall, calculated on each day since the resumption of observations in 1988. *Right:* As in left panel, extended back to 1898. Red points indicate where two or more consecutive dates were filled in using nearby station data.

Table 2. Significant drought events with 1-year rainfall below 500 mm, since records began. The third column gives the lowest 1-year cumulative rainfall total received in the period, and the second column is the Julian Date (JD) on which it occurred.

Calendar dates	JD	1-y cumu. rainfall mm	Name
1902 Aug – 1903 Apr	16072	313.3	Federation Drought
1919 Feb – 1919 May[1]	22013	481.0	
1940 Oct – 1940 Nov	29933	450.3	WW II Drought
1942 Jan – 1942 Mar	30440	442.5	WW II Drought
1980 Jun – 1980 Jun[2]	44367	496.0	
1983 Jan – 1983 Mar[2]	45354	466.4	
2018 Mar – 2018 Sep	58268	413.4[3]	

Table notes: [1]The dry spell continued for some months afterwards and dipped below 500 mm again a year later. [2]These observations are based on data imported from nearby stations, so should be treated with caution. They are consistent with contemporary accounts of low rainfall. [3]The final row is the present and continuing drought, with its deepest low on 30 May 2018.

those floods realistically develop or last over a period of about one week, perhaps supplemented by lesser amounts of rain over the same period.

For drought, we might institute a definition of less than half the annual rainfall to have fallen in any given 1-yr period. Only 4 such droughts have occurred, perhaps suggesting our definition is too extreme. Drought events are recorded in Table 2, where this definition is relaxed to 500 mm per year, resulting in two more such droughts. The most extreme of the six was by far the 1902–1903 "Federation Drought", not only in duration but also in its severity. Now, Jenolan Caves finds itself in a similar situation. The 2017-2018 drought is the second driest in recorded history for this location. Careful inspection of Figure 6 shows it has surpassed the once-in-25-years level and is a once-a-century drought. It has been 99 years since a drought has persisted for more than three months at this level. The present drought has not only persisted for longer, but is 15% drier than that event.

Under the definition above (<500 mm/yr), the 11 mm that fell on 8 Sep 2018 brought the present drought to an end with a 1-year cumulative rainfall of 503 mm, but in the absence of significant and frequent rainfall, drought conditions still persist at Jenolan Caves. The *in-situ* observations presented in Sect. 5 can still be expected at Jenolan Caves. In the next section, I investigate how recent climate change may have intensified the drought.

4 The role of temperature

Rainfall data do not tell the whole story. Increases in evaporation and transpiration, whatever the cause, intensify droughts. Since the global land-ocean temperature index has climbed markedly over the past 50 yr (Hansen and others 2010, GISTEMP Team 2018), corresponding increases in evaporation and transpiration will make droughts more severe in the modern era. In this section it is shown that the temperature at Jenolan Caves has increased significantly in recent decades.

Temperature data from the Jenolan Caves weather station are not available after 1973, and are often patchy before then. The nearby stations used for rainfall analysis in Sect. 3 also do not have adequate temperature data, so instead temperature data from the Katoomba Murri St station were used (see Table 1), as the nearest station with complete temperature records for the past half-century. The Jenolan Caves station is lower lying than the Katoomba station, so the stations are not expected to have the same temperature. Nonetheless, it is assumed that they have responded similarly to climate change and that decadal increases in temperature at Katoomba are representative of those at Jenolan Caves.

Figure 7 shows decadal changes in temperature since 1960 at Katoomba as a proxy for Jenolan Caves. For this, the average daily maximum for each day in each calendar month was taken, and averaged over the decade. Hence for the point at January for the 1960 decade, I took all (31x10=) 310 January days from the years 1960-1969, and calculated the mean temperature. The data for the 2010s show warming of 2°C compared to the next-warmest decade, and nearly 4°C compared to the 1960s. We show that average daily maximum temperatures this decade are at least 2 C warmer than in the previous century.

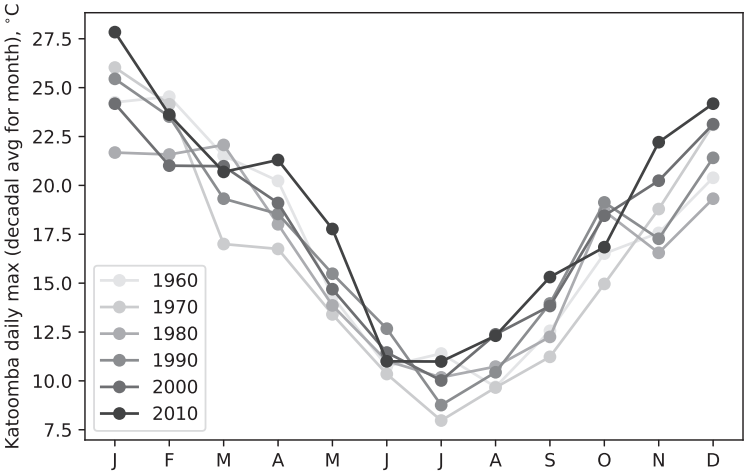

Figure 7. Decadal temperature comparisons for Katoomba, 29 km from Jenolan Caves, 'as the crow flies' . The data show a warming, particularly in the last two decades, that can be expected to exacerbate drought conditions.

5 In situ inspection

This article was prompted by visits to Jenolan Caves, where it was noted that several trips had gone by with little to no rain and the caves were getting drier between each visit. This section describes flow rates and water levels at points of interest in the hydrology of Jenolan Caves.

Volumetric flow rate observations were carried out by (i) selecting a length of stream where the cross-section is uniform, or as close to it as possible; (ii) estimating that cross-section; and (iii) measuring water flow speed. Where possible, the latter was done by dropping a floating object (e.g. a leaf) into the water and timing its passage between

the ends of the identified length of stream. With the cross-section and velocity, one obtains a volumetric flow rate. The nature of the measurement means that these flow rates should be considered as broad estimates only.

5.1 Watersend

Ordinarily the Jenolan River sinks into gravel to the north of Wiburds Bluff (Shannon 1976). Just to the north of the ruined Rowe Hut at the northern end of Rowe Flat (the largest alluvial flat, lying to the east of Wiburds Lake Cave), the gravel is capable of taking 45-60 l/s in each of three sinks. The northernmost of these was the main sink in the 1970s, but those were wetter times, as was shown in Figure 6. For most of the past ~25 yr, the main sink has been a pool opposite J244-245 Watersend Cave that is capable of draining 60 l/s.

On 2 Jun 2018 the stream had a very small flow near its terminus, no greater than 5 l/s, and was sinking at 33°46'56.15"S, 150°00'26.19"E in the middle of the flat that lies north of Rowe Flat (labelled '2018 terminus' in Figure 2). This is 600 m away from the 1970s main sink on a bearing of 325°, and it is 370 m on a bearing of 324° from the sink at Watersend Cave, both measured 'as the crow flies'. The stream lost its flow into the gravel over approximately 10–15 m of creek bed. The following month, on 12 Jul 2018, the stream was sinking 10 m down the valley from there with no noticeable change in creek flow rate further to the north. However, on this occasion, a very minor flow of ≲0.1 l/s was observed over a short section of creek bed where the creek first flows against the eastern edge of the valley floor (33°46'56.5'S, 150°00'29.3"E). The latter was not connected to the main stream via surface flow and the change in altitude of these creek sections is only 1 m over a horizontal separation of 70–100 m, suggesting that a resurgence is an unlikely explanation. The area was revisited on 7 Oct 2018 and the flow rates estimated again. They are compared on a map in Figure 8.

5.2 Imperial Streamway and Far Country

Between the third upstream sump and the second upstream sump, as labelled in the 1979 map by Lewis & Allum (Figure 9), I estimated the flow rate to be 50±20 l/s. While the second upstream sump is a duck-under, the third upstream sump (and the fourth, beyond it) require dive gear. The fifth upstream sump lies in a passage to the north-east of the Imperial Streamway, in Far Country. On 3 Jun 2018 it was observed to be a pool, rather than a sump, with a depth of 20 cm and a further 20 cm of airspace at the roof's lowest point. There was no flow between this 'sump' and the Imperial Streamway.

Following the passage further in the same north-easterly direction, two dive lines are encountered. The first passes through an area that is clearly sumped in wet conditions, as evidenced by high water marks on the walls and the installation of a dive line, but on 3 Jun 2018 was found to be mostly dry, with no pooled water though damp sediment lined the floor. The 6th upstream sump begins shortly beyond here, in the same location as indicated on the map, suggesting no substantial retreat in the present drought.

5.3 Mammoth Cave

Mammoth Cave has been thoroughly surveyed by Sydney University Speleological Society (SUSS), the maps from which can be found in *SUSS Bull*, 52(1), 52(3), 53(3) and 55(2) (Maynard 2013a,b, 2014, 2016). The cave has several watercourses including two rivers (Central River and Lower River), two major lakes (Ice Pick Lake and Slug Lake), and several pools and sumps. Together these offer a window into the hydrology of the Jenolan Caves system. The following observations have been made during the present drought.

- The southern part of Railway Tunnel, between Horseshoe Cavern and Skull and Crossbones, has dried considerably. Usually dominated by slippery wet mud and the occasional small puddle, the mud here is now firm.
- Central Lake is dry, with a sandy bed.
- Southbound (downstream), Central River usually sumps shortly after Central Lake. The river passage is currently dry and accessible for some 30 m south of the large Central Lake chamber, right until its southernmost surveyed location at station lake.cld14 (Maynard 2014), located at MGA (56H) 224128, 6255441, altitude 769 m. Immediately before the sump the sediment changes from sand to a fine-grained mud/sand mixture (Figures 10 and 11). It seems this area is accessible in moderately dry conditions, occasionally via a duck-under (Staraj 2004).
- Central River north of Central Lake and south of First Crossing is dry, and the river bed has thin calcite residue.
- Central River north of First Crossing is also completely dry with calcite deposition. There is no trickle from the Ninety Foot, down from Railway Tunnel.

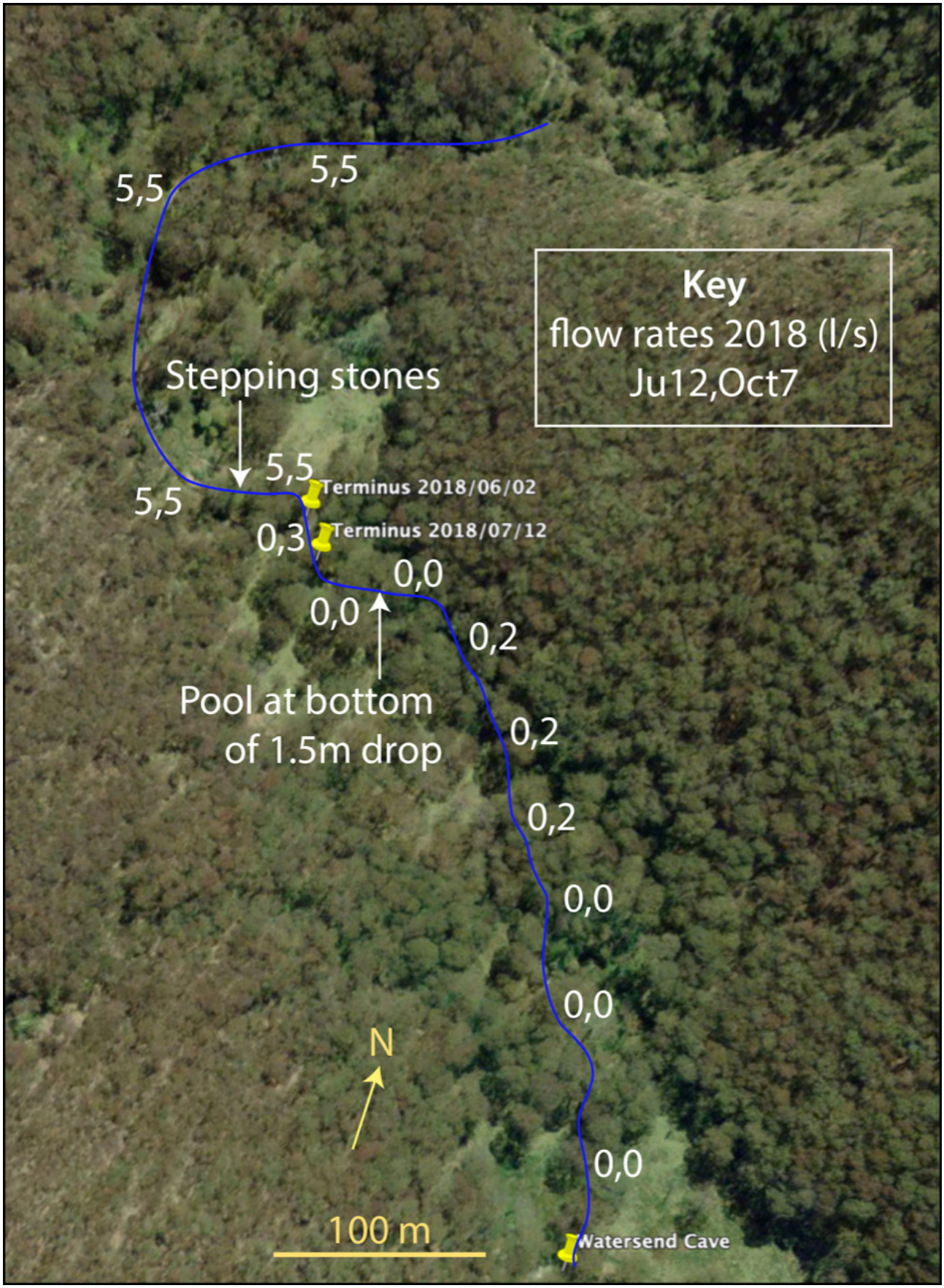

Figure 8. Map of the northern end of McKeowns Valley. The approximate river course is illustrated with a blue line, with the direction of flow being generally south. Flow rates along its course in l/s are written in white for two dates: 12 Jul 2018 and 7 Oct 2018. The two termini mentioned in-text are pinned with their corresponding dates, as is Watersend Cave in the south. The river leaves the slate at the position of the first flow estimate. Map imagery from NSW Globe, which is copyright of Department of Finance, Services & Innovation 2018.

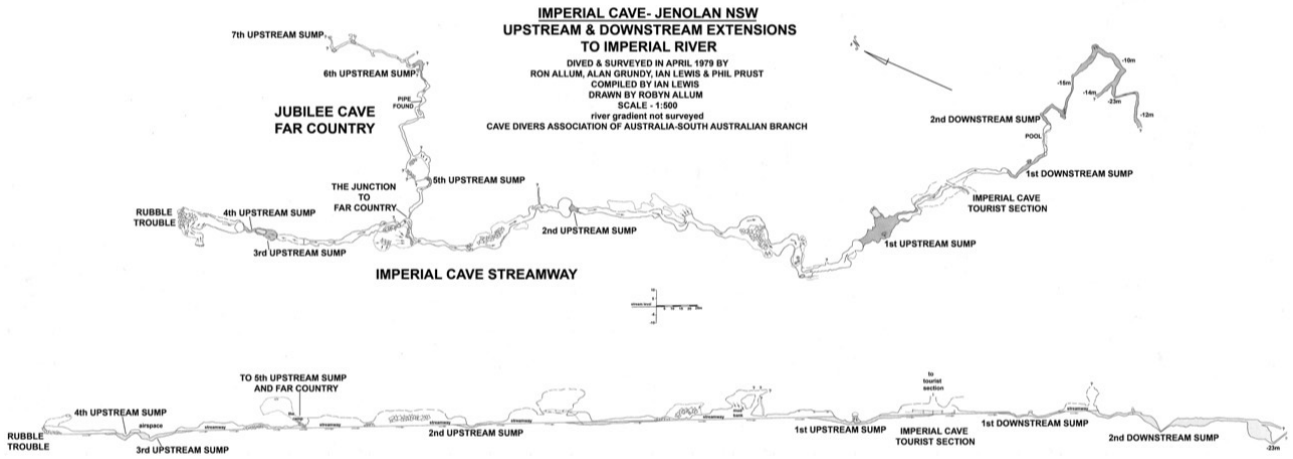

Figure 9. Map of the Imperial Streamway by Lewis & Allum from the SUSS map library.

Figure 10. Central River southern sump. The underwater photo (left) shows that the river passage continues in a tight phreatic tube. Photo credit: Rafid Morshedi. Date: 12 May 2018.

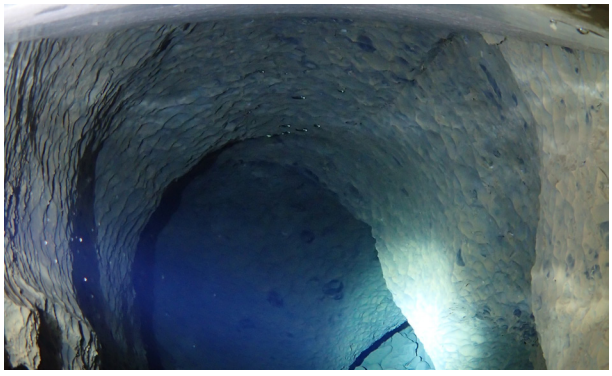

Figure 11. Central River southern sump, two months later. The water level is not visibly different from the photo in May. Photo credit: Rafid Morshedi. Date: 14 July 2018.

- The sump of Central River, just north of the First Crossing rockpile is also completely dry (Figure 12). Here, there is a 30 cm layer of sand, beneath which is some damp mud. The mud may dry if exposed to air.
- The Overflow Sump, which is the lowest part of Mammoth Cave except from Ice Pick Lake and Slug Lake, is dry and passable. Gravel is abundant either side and through the (dry) sump (Figure 13).

Figure 12. Central River, first sump north of First Crossing. No water was evident. Sand transitions to mud about 30 cm below the surface. Subject: Simon Murphy. Photo credit: Rafid Morshedi. Date: 12 May

- Between The Overflow and The Junction, south of Northwest Passage, there is normally a resurgence of Central River in a narrow hole in bedrock beneath a 3 m climb. This is also

Figure 13. The Overflow sump on Central River. No water was evident. Ample stream gravel was found and had to be removed to pass under the bedrock. Subject: Joshua Parker. Photo credit: Rafid Morshedi. Date: 12 May 2018.

dry. Gravel covers the floor. There are no new exploration opportunities here since the bedrock hole is too tight for humans (Figure 14).

Figure 14. The resurgence of Central River (impassable hole to lower right) contained no water. The ground is covered with gravel. Glove for scale. The dark area in the upper left is a shadow. Photo credit: Rafid Morshedi. Date: 10 Aug 2018.

- The Overflow is a tight phreatic tube with minor vadose modification. Stream gravel lines the floor, and water can drain through occasional fissures. There is no flow here at present (Figure 15). This only flows during floods.
- There is no water in The Liquidator, as far as this passage can be accessed by normal-sized humans (Murphy & Morshedi 2018). Progress here is hampered both by the twisting shape of the rift and its narrow size, before it descends steeply at similar dimensions (Figure 16). Since that visit, I have learned of an obscure but 'easier' route into The Liquidator which apparently leads to a 'squalid sump' (Staraj 2004) but I have not yet had the opportunity to revisit.

Figure 15. The Overflow also contained no water. Stream gravel in the floor was dry, but water can drain to lower levels through small fissures. Subject: Simon Murphy. Photo credit: Rafid Morshedi. Date: 14 Apr 2018.

Figure 16. The Liquidator contained no water. Central River was not flowing into this part of the cave. This passage could not be investigated much beyond the entrance of the rift. Subject: Rafid Morshedi. Photo credit: Rafid Morshedi. Date: 14 Apr 2018.

- Ordinarily Central River would flow from Risky Business to The Liquidator, but there is no flow at present.

- Risky Business is surprisingly wet, given the appearance of other areas of the cave. There are several small pools of clean water in the rock floor, filled to their brims. These appear to be supplied by water dripping from the roof, probably arriving via the nearby shale contact.
- Unlike Risky Business nearby, Damocles Lake is dry, with a sandy bed. The "muddy sump" described on the survey (Maynard 2016) is also dry, and this was pushed on a recent trip to a newly-entered sand-floored chamber (Murphy 2018).
- Waterfall Passage still carries its permanent trickle. This has never been observed to cease flowing.
- Dry Syphon is dry except for water emanating from Waterfall Passage, which then all exits Dry Syphon through a narrow slot in rock in the western wall. No water is flowing south out of Dry Syphon.
- No water is flowing or pooled in any significant quantities in Northwest Passage. Mud in the Guzaround area is still damp and soft.
- Sewerslide in Northwest Passage is the exception, still looking wet and uninviting as it must have when first named.
- Debouchment Detour usually contains one long muddy puddle and a smaller one to its southwest that sits in a constriction on a corner. The larger of the puddles still has its main body where the passage turns north, but it is narrower and shallower than usual. The northern end of this puddle is now heavily fragmented and most of the depth is soft mud, rather than water. The south-western puddle no longer exists.
- The small man-made dam just north-east of First Crossing was initially constructed for the Easter Camp of 1961 to collect drinking water where it constantly drips down here. It is now so empty that it cannot be relied upon as a source of drinking water. In normal conditions this overflows the dam.
- The "hole to water" heading down and north from Snakes Gut (just before Gravel Grovel) still contains water, at least 1 m deep (Figure 17). However, it has receded enough from its usual levels to reveal a passage leading off it to the south-east (towards Ice Pick Lake) that is usually submerged (Figure 18). This is probably a fossil level of Central River.

Figure 17. The hole to water in Snakes Gut, believed to be part of the sumped Central River. Approximate depth 1 m. The white wire may be old dive line. Photo credit: Stephanie Murphy. Date: 13 May 2018.

Figure 18. The newly exposed tube leading south-east from the hole to water in Snakes Gut. Dimensions are approximately 30 cm high by 30 cm wide. Photo credit: Stephanie Murphy. Date: 13 May 2018.

- Ice Pick Lake is well down on normal levels, but this lake can have quite a variable surface height and "normal" levels have not been precisely recorded, so a direct comparison is difficult. The surface is presently 1.5 m below the dive-line tie-off in the middle of the chamber. This tie-off is submerged in wet years and in flood. The lake is partially covered in calcite rafts (Figure 19).
- At the confluence of Central River and Ice Pick Lake, the lake is now low enough that the river and lake are disconnected by a mud bank. Central River is also covered in calcite rafts and sumps

5–10 m upstream of the lake (Figure 20), as indicated on the survey (Maynard 2014).

Figure 19. Ice Pick Lake is presently about 1.5 m below the dive-line tie-off. Subject: Jen Evans. Photo credit: Lisa Vitaris. Date: 13 May 2018.

Figure 20. Looking approximately west at the Central River sump. Ice Pick Lake lies just out of frame to the left (south). Photo credit: Simon Murphy. Date: 13 May 2018.

- The survey indicates two pools at the start of World of Mud (i.e. the low western part). From the top of the 4 m pitch that precedes them, the western of the two appears dry and the floor muddy. The eastern pool could not be assessed due to permit restrictions.* At least one of these pools has been entered during a previous dry period and no way on was found (Staraj 2004).
- Lower River is flowing, with very reduced flow (Figs. 21 and 22). Only the southern of the two holes in the western wall is conducting any water. A gravel bank blocks flow from the northern hole (Figure 21). The flow here is an upwelling from a sump under pressure that ordinarily delivers ~140 l/s. At the time of writing, the flow is down to 40±10 l/s – the lowest flow ever recorded.
- At the far side of Lower River, after the first climb down towards Slug Lake but before the second, there is a sump on the east, beyond an 8-m climb down. This is considered a linked backwater of Lower River, which when dived by Rick Grundy was found to continue in passage too tight for a diver (Grundy 2014). It was not re-inspected for this work.

Figure 21. Upper: Looking approximately north, a gravel bank separates the northern outflow from the main southern outflow from the western wall at Lower River.
Lower: As above, looking approximately south.
Subjects: Pete Baxter, Miriam Noble. Photo credit: Shaleen Patel. Date: 7 July 2018.

Figure 22. Upper: Looking approximately north-east, a further 5 m downstream, flow is low enough to observe cascades.
Lower: Looking approximately south-east, after the small cascades at the deeper part of Lower River.
Photo credit: Shaleen Patel. Date: 7 July 2018.

* Note added in proof: during Jan. 2019 the eastern 'pool' was observed to be completely dry and the hole ~8 m deep.

- A similar sump between Lower River and Slug Lake exists in rockpile and was dived by Brian Hebden with the same conclusion, that it is a backwater of the river (Cooper, pers. comm.). It was not re-inspected for this work, either.
- Slug Lake is well down on normal levels, with "Arse Rock" now protruding above the surface. Dave Apperley has observed that the restriction at -30 m is silting up. It is not clear if this is a direct result of lower flow in Lower River. Similar observations were made during Ron Allum's record -96 m dive (Ryan 2001).
- Grinning Monster Lake (altitude of ~775 m) is usually at the same level as Lower River, except in flood, so I have declined to inspect it.

5.4 J340 Enigma Cave

While this article is concerned with the Northern Limestone, it is worth reporting a fleeting observation of J340 Enigma Cave. This diveable cave was discovered in 2013, with an entrance 10 m above the dry Camp Creek riverbed. The start of the dive is just a couple of metres below the entrance and hence some metres above Camp Creek level (Anon. 2013). The water was found to persist for quite some time and its depth is at least 11 m with open leads (Larkins 2014). Explanations for the cave have been put forward by Cooper in the same article (Larkins 2014), that this is either a resurgence or an old flood swallet. We checked on the water level during the present drought. On 7 Jul 2018, J340 was found to be full of water, still.

6 Conclusions

Archival data have been used here to study rainfall at Jenolan Caves. The years 2017 and 2018 have seen a once-in-a-century drought, which is the second-driest period since rainfall observations began in 1895. It is also apparent that Jenolan Caves undergoes variations in rainfall on time-scales of decades: the period 1895–1940 was much drier than 1950–1975, and 1991–2018 was comparatively dry again. Temperatures this century are shown to be, on average, approximately 2°C warmer than the mid-20th Century, and through increased evaporation and transpiration rates this will exacerbate droughts, now and in the future.

Observations are presented on the water levels at Jenolan Caves, including the location of the surface stream sink, flow rates of underground rivers, and the levels of pools and sumps. There are marked changes consistent with the low rainfall. Lower River, the centrepiece of Jenolan Caves hydrology, is at its lowest flow ever recorded.

Acknowledgments

The author thanks Ian Cooper and Phil Maynard for discussions on geology, hydrology and Jenolan Caves, as well as comments on a draft of this article. He thanks SUSS for a thoroughly enjoyable first 18 months of speleology, and Rowena Larkins for her patience with beginners. He thanks the *SUSS Bull* editors, past and present, for their hard work in creating and collating this important documentation. He is grateful for the effort of the SUSS librarian for digitising older publications and maintaining the online catalogue. Finally, the author thanks Timothy Van Reeth for teaching him some basics in Python to get started with this project.

References

Anon. 2013 Project progress, Jenolan. *SUSS Bull,* 52(3): 1.

Branagan, G., Pickett, J. & Percival, I. 2014 Geology and geomorphology of Jenolan Caves and the surrounding region. *Proc. Linnean Soc. NSW*, 136: 99-130.

Cooper, I. 1990 Intrusive control of speleogenesis. *SUSS Bull,* 30(1): 21-24.

Cooper, I. 1998 Geology. *SUSS Bull,* 38(4): 27-29.

Cooper, I. 2010 Jenolan floods! *SUSS Bull,* 50(1): 13-18.

Cooper, I. & Staraj, M. 1996 Wiburds Cave hydrology and dye tracing. *SUSS Bull,* 36(1): 35-38.

Dunkley, J. 1976 A model of cave development [in] Welch, B.R. (ed.) *The Caves of Jenolan 2: The Northern Limestone*. Sydney Univ. Speleo. Soc., Sydney, Australia, p. 10.

GISTEMP Team 2018 GISS Surface Temperature Analysis (GISTEMP). NASA Goddard Institute for Space Studies. Dataset accessed 19-01-2018 at https://data.giss.nasa.gov/gistemp/.

Grundy, R. 2014 Exploratory diving in Mammoth Cave, Jenolan. *SUSS Bull,* 52(4): 14.

Hansen, J.R., Ruedy, M., Sato, M. & Lo R. 2010 Global surface temperature change. *Rev. Geophys.,* 48, RG4004.

Johnston, D. 2014 The Deep End. *SUSS Bull,* 53(1): 9-10.

Kelly, B. 1988 BSc (Hons) Thesis: The hydrogeology of the Northern Limestone, Jenolan

Caves, and related land management issues. Univ. of NSW.

Larkins, R. 2014 Sunday Southern Limestone. *SUSS Bull,* 52(4): 17.

Maynard, P. 2013a Mammoth survey – Part 1, Southern Section. *SUSS Bull,* 52(1): 10-43.

Maynard, P. 2013b Mammoth survey – Part 2, Railway Tunnel. *SUSS Bull,* 52(3): 15-51.

Maynard, P. 2014 Mammoth survey – Part 3, Naked Lady Chamber area. *SUSS Bull,* 53(3): 6-39.

Maynard, P. 2016 Mammoth survey – Part 4, Middle Bit and North West Passage. *SUSS Bull,* 55(2): 7-51.

Murphy, S.J. 2018 A Mammoth epic. *SUSS Bull,* 56(4): 10-12.

Murphy, S.J. & Morshedi, R. 2018 No adult supervision. *SUSS Bull*, 56(4): 5-9.

Ryan, G. 2001 Cave diving at Jenolan 1996-1998. *SUSS Bull*, 41(1): 21-24.

Shannon, H. 1976 Notes on geology, geomorphology & hydrology [in] Welch, B.R. (ed.) *The Caves of Jenolan 2: The Northern Limestone*. Sydney Univ. Speleo. Soc., Sydney, Australia, pp. 5-9.

Staraj, M. 1989 Jenolan: Where it never rains but floods! *SUSS Bull,* 29(2): 45-49.

Staraj, M. 2004 Mammoth erotica. *SUSS Bull,* 43(4): 14-21.

Vaughan-Taylor, K. & Ryan, G. 2000 Cave diving at Jenolan. *SUSS Bull,* 40(1): 36-46.

Welch, B. 1975 Some observations on the Jenolan flood, 21 Jun 1975. *SUSS Bull,* 15(8): 5-8.

Helictite, (2019) 45**:** 27-37

Are the orthoquartzite towers and caves on the Borradaile Plains, Tasmania, formed by dissolution and arenisation?

***Adrian Slee*[1] *and Peter D. McIntosh*[1]**

[1]Forest Practices Authority, 30 Patrick Street, Hobart, Tasmania 7000, Australia
adrian.slee@fpa.tas.gov.au

Abstract

The discovery of significant cave and karst landscapes formed in quartzites and sandstones in South America, Africa and Australia has led to a debate among scientists over the definitions of karst and the processes forming karst in quartzites. In the past these caves were listed under the ambiguous definition of 'pseudokarst' landforms. It is now generally agreed that the chemical dissolution of silica within massive quartzite or sandstone units plays a significant role in the development of certain types of quartzite caves and the term syngenetic karst may better describe non-carbonate landscapes where dissolution and sediment transportation by erosion processes both play major roles in karst development. The recent discovery of towers formed within Precambrian orthoquarzite rock adjacent to Tertiary basalt on the edge of the Borradaile Plains in northern Tasmania poses questions regarding the processes of quartzite dissolution and karst development in silica rich rocks in an area that has had a subalpine or glacial climate for much of the Quaternary. It is suggested that the overlying basalt has been stripped from around the towers by Quaternary erosion and the caves have formed by arenisation induced by acidic upland soils.

Introduction

In the scientific literature, karst has been recognised by landforms produced by the dissolution of carbonates (Ford and Williams 2007). However; recent studies of major karst landscapes containing sizeable caves formed in quartzite and sandstones (Piccini and Mecchia 2009; Uagoda and others 2011; Wray and Sauro 2017) have challenged this definition. For example the discovery of very extensive cave systems formed in quartzite and associated meta-sedimentary rocks including the 300 m deep Sistema Auyantepuy Noroeste (Piccini 1995) and Guacamaya Cave (Sauro and others 2013) on the Tepuis of northern South America and documentation of other significant quartzite karst areas in southern Africa (Marker and Swart 1995; Fabri and others 2015) and northern Australia (Grimes and others 2011) has made clear that over long time periods quartzites can produce karst landscapes. The most impressive quartzite karst landscapes in Australia are extensive tower karst and "ruined city" landscapes widely distributed across the Australian tropics (Young 1987; Wray 1997a; Grimes and others 2011), which display many landforms formed by dissolution such as pinnacles, street and block landscapes, and caves including the impressive 300 m long Whalemouth Cave in the Kimberley (Jennings 1983; Young 1987; Grimes and others 2011). Drainage conduits including caves several tens of metres long in sandstone have been described in the Carnarvon Gorge area of central Queensland (Wray 2009). Elsewhere, outside the tropics, small meander cut-off caves including the Underground River and Ross Cave formed in Sydney basin sandstone sequences have been identified as largely formed by karstic processes (Wray 1995, 1997; Dunkley 2011). The largest caves formed in siliceous rocks in Tasmania are Wet Cave near Sisters Beach on the north coast (Kiernan 1995) and Iron Maiden and Blister caves on the south-western coast of King Island in Bass Strait (Goede and others 1979). These caves have passages up to 120 m long. However, they are raised sea caves eroded in quartzite and are not of karstic origin, although carbonate speleothems derived from overlying dune limestones are present in the King Island caves (Goede and others 1979). Away from the coast in southwest Tasmania small quartzite fissure caves have formed on the Frenchmans Cap Range (Kiernan 1995) and have been observed by the primary author on the Needles Ridge near Maydena. At Mt Wright two large arches have formed in Ordovician sandstone and conglomerate (Middleton 2015). Like the previous examples none of these features appear to be of karst origin, but near Quamby Bluff on the lower slopes of the Great Western Tiers in northern Tasmania a cluster of caves formed in Triassic sandstone display some characteristics of solution weathering (Middleton and Sharples 2014). This paper describes newly discovered caves and associated surface landforms formed in orthoquartzite on the Borradaile Plains in northern Tasmania and discusses their mode of formation.

Study area

The Borradaile Plains, an extensive dolerite-capped plateau at 800–900 m above sea level (asl), form the drainage divide between the deep glaciated troughs of the Forth Valley to the west and the Mersey Valley to the east (Colhoun and others 1996) (Figure 1). The plateau is mostly underlain by a sill of flat-lying dolerite and areas of Tertiary basalt. However small areas of Precambrian basement documented on 1:250000 geologic maps outcrop as greenschist-quartzite sequences and related rocks around the perimeter of the plateau, particularly at its northern end (Mineral Resources Tasmania 2010). The study site is located on a westerly facing spur of the Borradaile Plains at an elevation of 810–840 m asl immediately upslope and east of the steep defile of the Borradaile Creek gorge that drops 400 m to the floor of the Forth Valley. Most of the Borradaile Plains have only been geologically mapped at a reconnaissance scale and the study site is mapped as greenschist quartzite rocks. However, during a field reconnaissance vesicular basalt of probable Tertiary age was noted immediately southeast of the study site where it forms two bedrock benches clearly visible on the hillshade map of the site (Figure 1). In the south of the study area flows of vesicular basalt are found on top of, and adjacent to, quartzite outcrops.

The Forth Valley has a temperate maritime climate with short mild summers. The nearest weather station of comparable elevation is at Waratah, 56 km west of the site, at 609 m asl. Here summers are short and mild with temperatures rarely rising above 30°C and winters are cold with average daily minimums of 0–2°C (BOM 2017a). On the Borradaile Plains temperatures are likely to be lower. Precipitation is around >1500 mm a year based on data from the Liena (Old School House) weather station 10 km to the northeast (BOM 2017b). Heavy snowfalls are common during winter. The natural vegetation cover is cool-temperate wet forest dominated by *Eucalyptus delegatensis* and shrubby grasslands. During the most severe glacial periods the Borradaile Plains may have been overrun by the extensive central plateau ice cap (Hannan and Colhoun 1987; Kiernan and Hannan 1991; Colhoun and others 1996). During the less severe last glaciation the Borradaile Plains were probably treeless with low alpine grasses and herb fields (Colhoun 2000; Hopf and others 2000). Under significantly colder but drier climates than at present the Borradaile Plains would have experienced extensive landscape

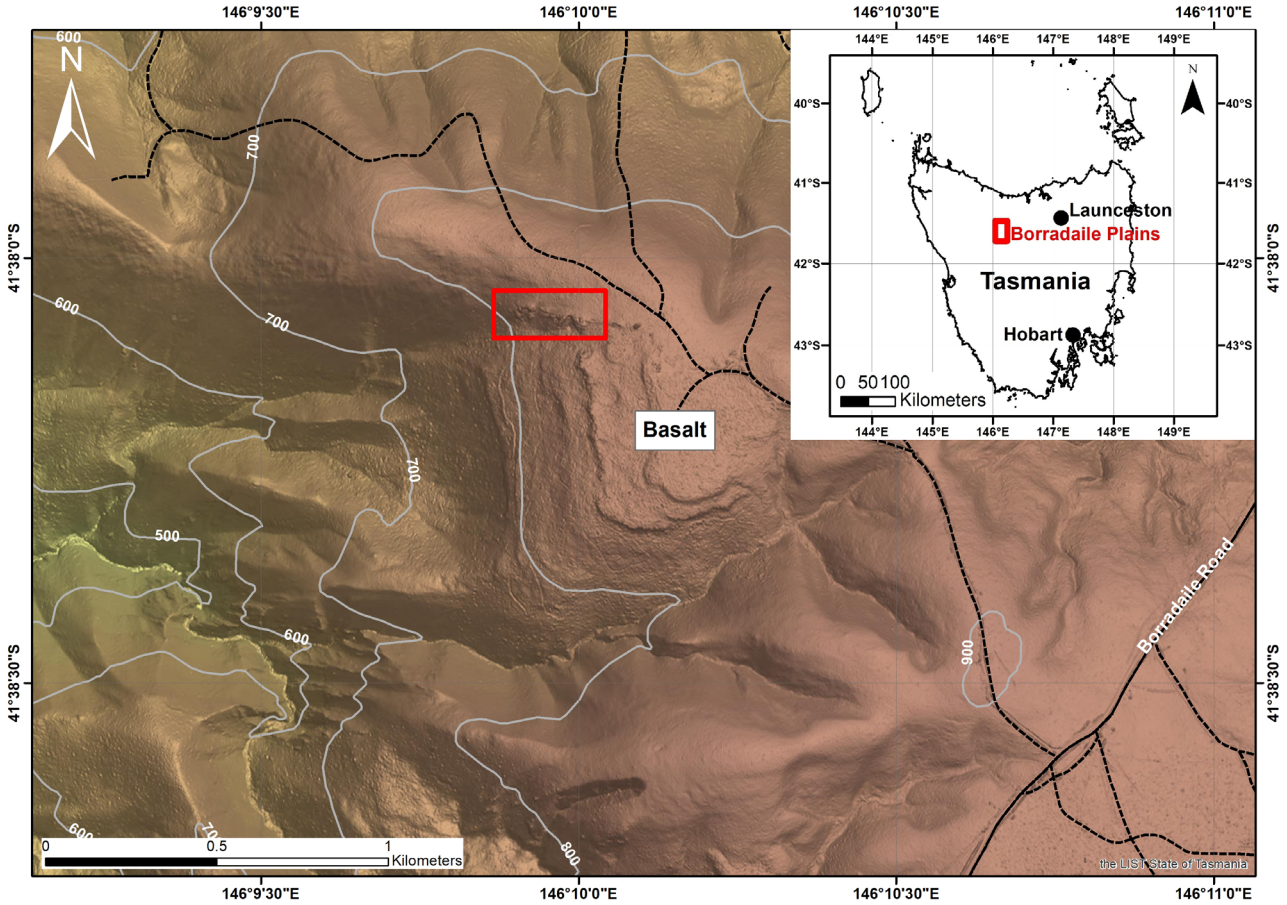

Figure 1. Location map and hill shade (LiDar-derived) map available on LIST Tasmania (https://maps.thelist.tas.gov.au/listmap/app/list/map), showing the topography in the immediate vicinity of the towers and study area (red outline). The towers and the flat lying basalt flows capping the plateau are prominent features in the landscape.

modification by periglacial processes such as frost shatter, solifluction and nivation (snow melt) (Slee and Shulmeister 2015).

The study site covers an area of approximately 3 ha enclosing a line of massive rock towers that rise steeply above the surrounding surface and resemble small "ruined city" forms common in tropical quartzite areas such as those described in the Northern Territory (Grimes and others 2011). The two main outcrops have been designated the East and West towers and contain most of the major karst features. However, karst landforms are also present within the smaller isolated towers. The towers are composed of folded massive orthoquartzite beds separated by schistose units.

Methods

The study area was surveyed in 2011 using compasses and tape measures by the authors with the aim of developing a sketch map of the landforms and listing the landforms present, so that management plans for an adjacent forest coupe could be developed and a proposal written for future listing of the landforms on the Tasmanian Geoconservation Database (TGD), which formally recognises sites of geoconservation significance in Tasmania (Comfort and Eberhard 2011; DPIPWE 2019). This site was formally listed on the TGD in April 2018. In February 2016 a bushfire burnt through the site and destroyed the vegetation. Consequently, the initial survey was updated in 2017 and the impacts of the bushfire on the caves detailed (Slee 2017).

Description

The outcrops extend east-west for 300 m on the top of a south-west facing spur of the Borradaile Plains. The two main towers are surrounded by steep cliffs up to 8 m high and rise up to 12 m above the surrounding undulating plains (Figures 2 and 3). The towers are surrounded by smaller outliers that rise abruptly up to 4 m above the land surface. Unlike typical scarp-retreat cliff faces that form cliffs and drop-offs at the edges of plateaus as a result of weathering and cliff face collapse, the towers rise above the surrounding landscape on all sides. The linear trend of the outcrops striking to the west-north-west suggest that they may be the remnants of a single hogsback strike ridge that projected above the general elevation of the Borradaile Plains.

Karst landforms are common throughout the study area. Landforms identified include numerous grikes and solution hollows in the base of the cliffs, rudimentary sinkholes on the summit area of the eastern tower and small enterable caves.

Surface landforms

The towers have steep cliff-lined profiles with massive smooth walls and rugged domed to turreted summits (Figure 4). No karren were observed on the towers; however the East Tower is broken by large smooth bedrock ridges with the result that the quartzite projects several metres out from the tower. These landforms are reminiscent of karst grike fields in Ordovician limestone outcrops observed elsewhere in Tasmania.

No sinkholes were observed on the plateau surrounding the outcrops but several small circular bedrock depressions up to 1.5 m deep occur on the upper part of the East Tower in the vicinity of cave 5 and at the far eastern end of the mapped outcrop.

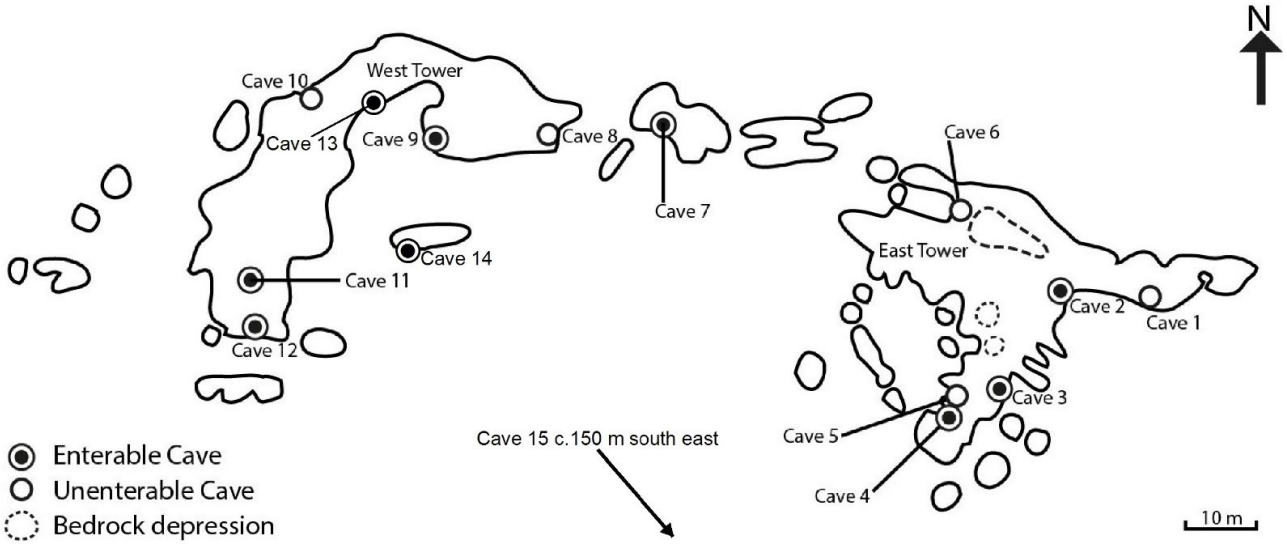

Figure 2. Map of the quartzite towers derived from detailed field mapping and observations.

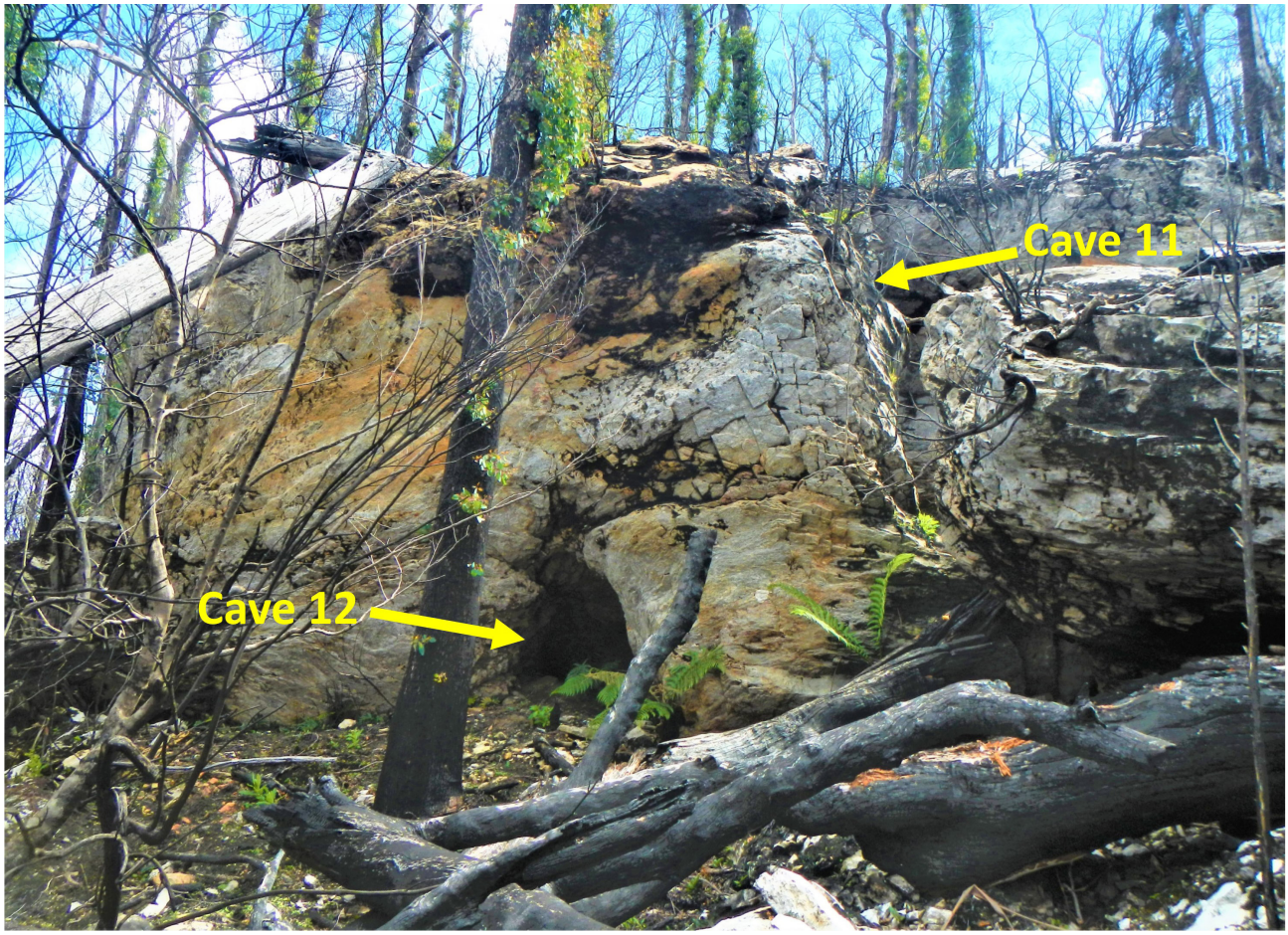

Figure 3. View of the southern face of the western tower, caves 11 and 12 are arrowed.

Figure 4. The rounded summit of the western tower.

Although many of the outlying towers appear to be formed in solid bedrock some large boulders are present down slope of the towers, hinting at past tower collapse. Two notable cave-collapse features are present in the East Tower. Cave 4 appears to be a former tunnel cave with a partially collapsed outer wall, which has promoted development of an unstable breakdown area. A 6 m long and 2 m deep grike is a major feature of the western end of the East Tower. The straight walls of this feature, the large angular talus blocks lying on the floor of the grike and a tight 5 m long cave passage (cave 6) at the end of the grike, all suggest that this feature formed by roof collapse of a more substantial cave. In contrast to the East Tower, the West Tower presents a massive profile with straight-sided vertical to overhanging cliffs up to 8 m high and no surface sinkholes. Grikes are only weakly developed. The most notable surface landforms on the summit of the West Tower are a series of 2-3 m tall rounded summit tors.

Caves

Fifteen caves were located; of these eleven were accessible. Six caves are located within the East Tower, six within the West Tower and three are located in outlying smaller bedrock bluffs. The caves have been divided into three categories:

Tube (Figure 5): Single or double rounded tunnels that end in pools of water. These caves appear to be subsurface continuations of surface grikes penetrating the edges of the towers. Four caves display this morphology, and two of these are >10 m long; all contained small standing pools of water in their inner reaches during visits in 2011, but were dry during the 2017 observations after the bushfire. The presence of standing pools of water coupled with these caves' rounded phreatic style of development suggest that these caves may have formed by the slow dissolution of quartzite by ponded rainwater acidified by the organic-rich upland soil. This deduction is supported by the observations of Hill and others (1995, p. 283) that soils formed in Ordovician quartzites in the Forth region have extremely acid peaty topsoils of pH 3.8, and subsoils have pH of 4.5. In addition, Bennett and others (1988) demonstrated that dissolution of quartz in water is greatly accelerated by the presence of organic acids. Dissolution is likely to have been initially associated with pits in the bedrock surface and over time developed along grikes and elongated tunnel caves. In cave 9 a seepage displays well developed runnels and small stalactites are present on the nearby roof (Figure 6).

Figure 5. View towards the back of the tube-shaped passage of cave 9.

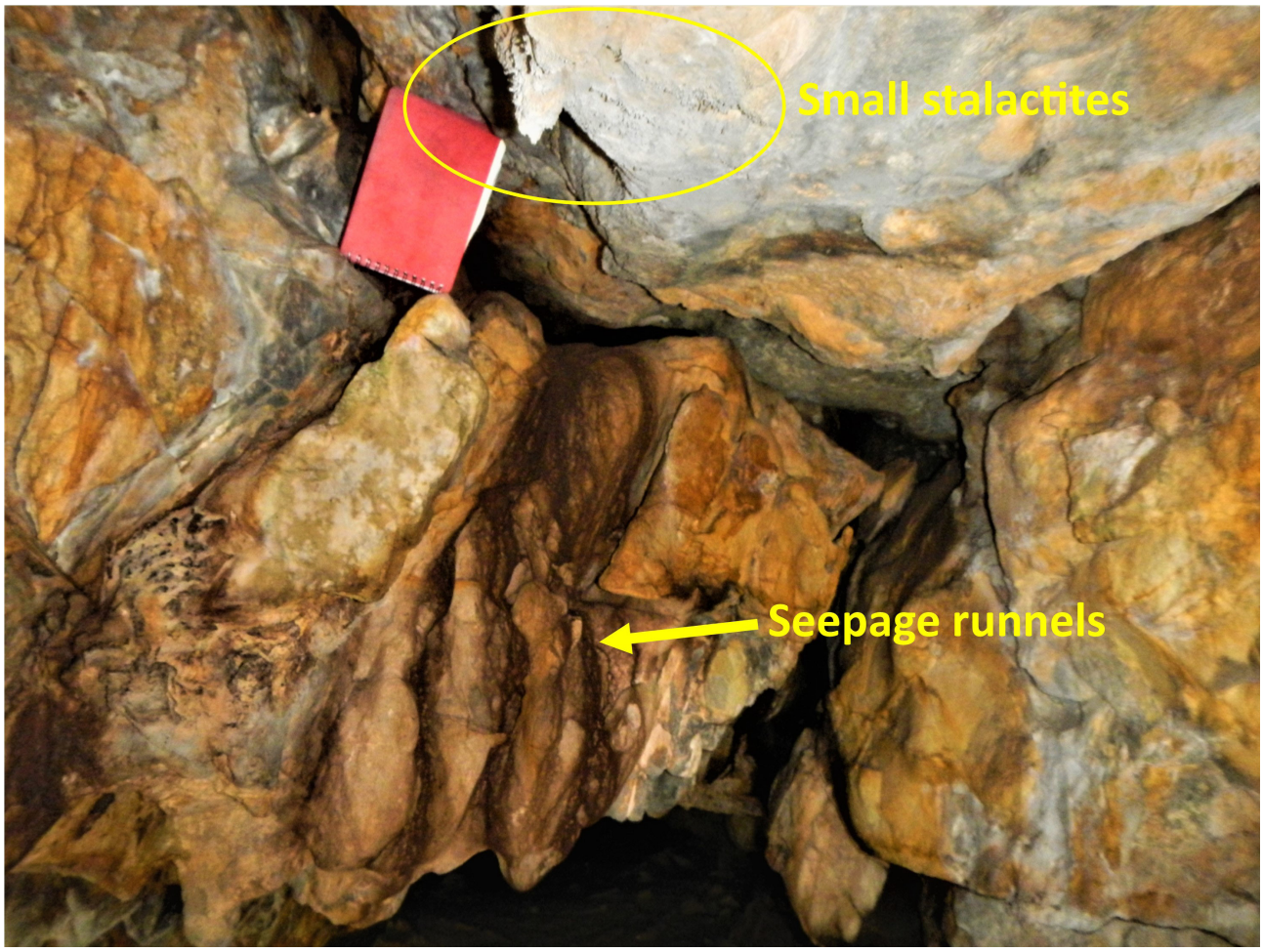

Figure 6. Location of small seep and solution runnels (arrowed) in the roof of cave 9. Also note miniature stalactites adjacent to the note book. The seep dried up after the 2016 bushfires.

Wide and low (Figure 7): Caves with wide passages have formed at the soil/bedrock contact. Caves 7 and 14 feature low tight entrances leading to more extensive low tent-shaped passages of unknown length. These caves have similar morphology to that of caves formed by basal dissolution of tropical karst towers by surrounding swamps, producing "swamp notches" (McDonald and Twidale 2011). Cave 12 on the West Tower appears to have a similar origin however it has an inner chamber 2.5 m tall.

Open tunnels (Figure 8): Cave 11 is a single 2.5-3.5 m tall arch in the West Tower and forms an 11 m long walk-through cave. No pools were observed in this cave. The cave follows a structural weakness in the bedrock (a band of thin schistose beds) and the cave probably developed along this weakness. Cave 15 lies within a small outlying bedrock bluff (not shown in Figure 2); it features approximately 10 m of passage that extends the width of the bedrock outcrop and features three entrances to a small inner chamber.

It is notable that the caves appear at two elevations within the towers; the swamp-notch caves lie topographically below other caves. This difference in elevation is most obvious in the West Tower in which the entrance of cave 12 lies 2-3 m below the base of cave 11 and cave 12 has a N-S passage alignment as compared to the E-W alignment of cave 11.

Discussion

Caves formed in quartzite and sandstone bedrock in Tasmania are usually formed by mechanical processes. The most common process for forming caves in sandstone is wind erosion or less commonly landslides and localised slope unloading processes (see Sharples 1997) or caves possibly associated with fault zones (e.g. Slee and Stoios 2019). In drier and coastal parts of the state, salt weathering is likely to be a factor in the mechanical breakdown of sandstones (Rodriguez-Navarro and others 1999) and may play a role in the formation of tafoni on cliff faces in eastern Tasmania (Williams 2007). Sharples (1990) notes that salt weathering is more prevalent in sandstones containing clay minerals rather than in sandstones composed purely of quartz. Salt weathering is unlikely to be active on the high-rainfall Borradaile Plains or to affect indurated orthoquartzite and is discounted as a process forming the described

Figure 7. Left, The low entrance to cave 14 (circled) with the main West Tower beyond. Right, View into the western passage of cave 14. This passage extends for at least several metres out of sight. Note the lack of coarse rubble on the floor of the cave, as in cave 3 (Figure 9). We suggest this cave formed as a void partially or wholly filled with acid soil, and that it is slowly being exhumed.

Figure 8: Cave 11 is an 11 m long and 3-4 m high tent-shaped passage. Note the recent angular shards of rock at the entrance and burnt eucalypt produced by the intense bushfires that impacted the site in January 2016

landforms. Caves formed elsewhere in Tasmania due to mechanical weathering processes generally have breakdown deposits on their floors and angular faceted walls resulting from the mechanical fracturing of beds within the host rock. In contrast the caves on the Borradaile Plains have vegetated soil-covered floors with smooth walls and limited evidence of breakdown (Figure 9).

An alternative process for cave formation at Borradaile is slow dissolution of quartz along rock fractures by meteoric water, generally in the soil saturation zone, a process widely accepted as initiating quartzite caves and known as arenisation (Piccini and Mecchia 2009; Grimes and others 2011; Sauro and others 2012; Sauro 2014; Wray and Sauro 2017). Dissolution and preferential breakdown of massive quartzite occurs along lines

Figure 9. Left: The twin entrances to cave 3 are separated by a column. Note these entrances lie on the sheltered easterly aspect of the Eastern Tower which is not exposed to the prevailing westerly winds. Right: Back passage of cave 3, note the smooth rounded walls of this passage.

of weakness in the rock to form voids of loose sands and remnant silcrete. If the overlying soil is removed, physical weathering processes including wind deflation and stream/water erosion can rapidly remove the loose grains in the rock mass leading to cave formation (Wray 1997b; Grimes and others 2011; Sauro 2014). If feldspars are present in sandstones or quartzite their chemical breakdown under acidic meteoric weathering regimes may also be a factor (Aubrecht and others 2011, 2013).

In Australia, karst development in quartzite has been mostly documented in tropical and sub-tropical environments and within the humid temperate zone (with warm to hot summers and mild winters) in Sydney basin sandstones (Wray 1995, 1997; Dunkley 2011). The climates there are significantly different from the cool-temperate Borradaile Plains. The processes that formed caves within the Fell Sandstone of Northumberland Britain (Self and Mullan 2005) may provide a closer analogue for conditions that formed the caves on the Borradaile Plains. Several small caves in the Fell Sandstone appear to have formed by arenisation: the largest is the 10 m long Routin Lynn Cave that has a similar morphology to a number of the caves present on the Borradaile Plains. Self and Mullan (2005) postulated that surface karst landforms and most of the caves they describe must have formed since the retreat of the Younger Dryas ice cap that buried the area 13,000 years ago, and that most features in the Fell Sandstone developed rapidly during the warmer, more humid, Holocene.

The juxtaposition of Precambrian quartzite and Tertiary basalt immediately east of the towers hints at a process that may have produced the rounded quartzite outcrops. In the past the host quartzite bluff is likely to have been buried by basalt (Figure 10). The deeply incised but rounded nature of the quartzite outcrops contrasts to the elongated sharp quartzite ridges visible on the shade map downslope in the Borradaile Gorge, and suggests that most or all of the outcrops may have once been buried by weathered basalt. We note that the Tertiary climate was warmer than at present and the pH of deep subsoils may have been higher than in present-day basaltic soils due to faster mineral weathering rates. Quartz dissolution is quicker in high pH solution than in low pH solution (Henderson and others 1970) so leaching of the quartzite by water percolating through basaltic soils could have formed much of the rounded topography of the quartzite outcrop.

Summary

Most quartzite and sandstone caves showing evidence of dissolution and arenisation in Australia are located in tropical or sub-tropical environments but the caves in orthoquartzite on the Borradaile Plains are in a cool temperate climate that would have been sub-alpine or alpine in character throughout much of the late Quaternary. We suggest the landforms evident today have been formed by two processes. During the Tertiary the underlying quartzite was weathered by high pH solutions percolating through deep weathered basalt, forming the rounded topography of the outcrop we see today. Subsequently, chemical weathering by acid soil solutions rich in organic acids and arenisation processes have eroded caves at soil level. At present

Figure 10. One of the entrances to cave 15. The GPS lies on a boulder of vesicular basalt of likely Tertiary age that lies immediately upslope of the quartzite outcrop where it forms a low escarpment.

many caves are found near the present soil surface, but caves higher in the outcrop may have formed when the soil surface was higher, i.e. the outcrop and its caves are slowly being exhumed by erosion driven by cold-climate processes, fire, ground ice and sheet wash.

The recent discovery in north western Tasmania of the Borradaile towers and associated landforms indicative of karst processes are significant not only for their geomorphic isolation from similar landforms but also for their deduced mode of development in a region that has been heavily modified by glacial and periglacial processes throughout the Quaternary. The authors support the notion that the Borradaile towers and caves are primarily of solution origin and therefore should be classified as karst rather than 'pseudokarst', as discussed by Eberhard and Sharples (2013).

Acknowledgements

The authors thank Sustainable Timbers Tasmania (formerly Forestry Tasmania) for granting access to the site, Forest Practices Officer John Tabor who accompanied A. Slee on the first site visit during coupe planning and Rolan Eberhard (Department of Primary Industries, Parks, Water and the Environment) who read the paper and provided feedback.

References

Aubrecht, R., Lánczos, T., Gregor, M., Schlögl, J., Šmída, B., Liščák, P., Brewer-Carías, Ch. and Vlček, L. 2011 Sandstone caves on Venezuelan tepuis: return to pseudokarst? *Geomorphology,* 132: 351-365.

Aubrecht. R., Lánczos. T., Gregor, M., Schlögl. J., Šmída. B., Liščák. P., Brewer-Carías. Ch. and Vlček. L. 2013 Reply to the comment on "Sandstone caves on Venezuelan tepuis: Return to pseudokarst?" *Geomorphology,* 197: 197-203.

Bennett, P.C., Melcer, M.E., Siegel, D.I. and Hassett, J.P. 1988 The dissolution of quartz in dilute aqueous solutions of organic acids at 25°C. *Geochimica Cosmochimica Acta,* 52(6): 1521–1530.

Bureau of Meteorology 2017a Daily minimum temperature Waratah (Mount Road). http://www.bom.gov.au/jsp/ncc/cdio/weatherData/av?p_nccObsCode=123&p_display_type=dailyDataFile&p_startYear=2001&p_c=-1882423953&p_stn_num=097014 accessed 8/8/17.

Bureau of Meteorology 2017b Monthly rainfall Liena (Old School House). http://www.bom.gov.au/jsp/ncc/cdio/wData/wdata?p_nccObsCode=139&p_display_type=dataFile&p_stn_num=091151 accessed 8/8/17.

Colhoun, E.A. 2000 Vegetation and climate change during the Last Interglacial-Glacial cycle in western Tasmania, Australia. *Palaeogeography, Palaeoclimatology, Palaeoecology,* 155(1-2): 195-209.

Colhoun, E.A., Hannan, D. and Kiernan, K. 1996 Late Wisconsin glaciation of Tasmania. *Papers and Proceedings of the Royal Society of Tasmania,* 130(2): 33-45.

Comfort, M. and Eberhard, R. 2011 The Tasmanian Geoconservation Database: A tool for promoting the conservation and sustainable management of geodiversity. *Proceedings of the Linnean Society of New South Wales,* 132: 27.

Department of Primary Industries, Parks, Water and Environment (DPIPWE). Tasmanian Geoconservation Database. https://dpipwe.tas.gov.au/conservation/geoconservation/tasmanian-geoconservation-database accessed 5/4/19.

Dunkley. J. 2011 Sandstone karst and caves – with particular reference to the Blue Mountains, NSW. Paper presented at 28th Biennial Conference of the Australian Speleological Federation, Chillagoe, Qld.

Eberhard, R. and Sharples, C. 2013 Appropriate terminology for karst-like phenomena: the problem with 'pseudokarst'. *International Journal of Speleology* 42(2): 109-113.

Fabri, F.P., Auler, A.S., Calux, A.S., Cassimiro, R. and Augustin, C.H.R.R. 2015 Cave morphology and controls on speleogenesis in quartzite: The example of the ItambÉ do Mato Dentro area in southeastern Brazil. *Acta Carsologica,* 44(1): 23-35.

Ford, D. and Williams, P. 2007 *Karst Geomorphology and Hydrology*. John Wiley & Sons Ltd, Chichester, UK. 562 p.

Geode, A., Harmon. R. and Kiernan. K. 1979 Sea caves of King Island. *Helictite,* 17(2): 51-64.

Grimes, K., Wray. R., Spate. A and Household. I. 2011 Karst-like and ruiniform features in sandstone in tropical Australia. Paper presented at the 28th Biennial Conference of the Australian Speleological Federation, Chillagoe, Qld.

Hannan, D.G. and Colhoun, E.A. 1987 Glacial stratigraphy of the Upper Mersey Valley, Tasmania. *Geographical Research,* 25: 36-46.

Henderson, J.H., Syers, J.K. and Jackson, M.L. 1970 Quartz dissolution as influenced by pH and the presence of a disturbed layer. *Israel Journal of Chemistry,* 8: 357-372.

Hill, R., Laffan, M. and Grant, J. 1995 Soils of Tasmanian State Forests. *Soils Bulletin* 3. Forestry Tasmania, Hobart. 317 pp.

Hopf, F.V.L., Colhoun, E.A. and Barton, C.E. 2000 Late-glacial and Holocene record of vegetation and climate from Cynthia Bay, Lake St Clair, Tasmania. *Journal of Quaternary Science,* 15(7): 725-732.

Jennings, J.N. 1983 Sandstone pseudokarst or karst? *Aspects of Australian Sandstone Landscapes. Australian and New Zealand Geomorphology Group Special Publication* 1: 21-30.

Kiernan, K. 1995 *An atlas of Tasmanian Karst, Volume 1*, Tasmanian Forest Research Council Inc. Research Report No. 10, p. 150.

Kiernan, K. and Hannan, D. 1991 Glaciation of the upper Forth River catchment, Tasmania. *Australian Geographical Studies,* 29(1): 155-173.

Marker M.E. and Swart P.G. 1995 Pseudokarst in the Western Cape, South Africa: Its palaeoenvironmental significance. *Cave and Karst Science,* 22(1): 31-38.

McDonald, R.C. and Twidale, R.C. 2011 On the origin and significance of basal notches or footcaves in karst terrains. *Physical Geography,* 32(3): 195-216.

Middleton, G. 2015 Mt Wright Arch GH1-2, Vale of Rasselas. *Speleo Spiel*, 414: 5-9.

Middleton, G. and Sharples, C. 2014 A group of unusual sandstone caves in northern Tasmania. *Journal of the Sydney Speleological Society,* 58(8): 211-222.

Mineral Resources Tasmania 2010 1:250,000 Digital Geology. Hobart, Tasmania. http://maps.thelist.tas.gov.au/listmap/app/list/map accessed 8/8/17.

Piccini, L. 1995 Karst in siliceous rock: karst landforms and caves in the Auyan-tepui (Est. Bolivar, Venezuela), *International Journal of Speleology,* 24(1-4): 41-54.

Piccini, L. and Mecchia, M. 2009 Solution weathering rate and origin of karst landforms and caves in the quartzite of Auyan–tepui (Gran Sabana, Venezuela). *Geomorphology,* 106(1-2): 15-25.

Rodriguez-Navarro, C., Doehne, E. and Sebastian, E. 1999 Origins of honeycomb weathering: The role of salts and wind. *GSA Bulletin,* 111(8): 1250-1255.

Sauro, F. 2014 Structural and lithological guidance on speleogenesis in quartz-sandstone: Evidence of the arenisation process. *Geomorphology,* 226: 106-123.

Sauro, F., Piccini, L., Mecchia, M. and De Waele, J. 2012 Comment on "Sandstone caves on Venezuelan tepuis: Return to pseudokarst?" by R. Aubrecht, T. Lánczos, M. Gregor, J. Schlögl, B. Smída, P. Liscák, Ch. Brewer-Carías, L. Vlcek. *Geomorphology,* 132: 351-365.

Sauro, F., Lundberg, J., Waele, J.D., Tisato, N. and Galli, E. 2013 Speleogenesis and speleothems of the Guacamaya Cave, Auyan Tepui, Venezuela [in] Filippi, M. & Bosák (eds) *16th Int. Congress of Speleology Proceedings,* Vol. 3: 298-304.

Self, C.A. and Mullan, G.J. 2005 Rapid karst development in an English quartzitic sandstone. *Acta Carsologica*, 34(2): 415-424.

Sharples, C.E. 1990 The durability of Tasmanian building sandstones. Unpub. Msc thesis, Geology Department, University of Tasmania, Hobart. 464 p.

Sharples C. 1997 *Bedrock dilation features at Diogenes Creek, Styx Valley.* A Reconnaissance of landforms and geological sites of geoconservation significance in the Western Derwent Forest District. A Report to Forestry Tasmania. Appendix 1.0, pp.113-114

Slee, A. 2017 Impacts of the 2016 bushfires on forest and caves at the Borradaile Plains. *Forest Practices News,* 13(3): 6-7.

Slee, A. and Shulmeister, J. 2015 The distribution and climatic implications of periglacial landforms in eastern Australia. *Journal of Quaternary Science,* 30(8): 848-858.

Slee, A and Stoios, A. 2019 An unusual polygenetic cave: Fishers Tier Cave, Ben Lomond, Tasmania. *Speleo Spiel*, 430: 23-26.

Uagoda, R., Avelar, A. and Netto, A.L.C. 2011 Karstic morphology control in non-carbonate rocks: Santana Basin, middle Paraiba do Sul river valley, Brazil. *Zeitschrift für Geomorphologie,* 55(1): 1-13.

Williams, B. 2007 *Analysis of the effect of excessive damp and chlorides on the sandstone walls of the Oatlands Gaol (1837)*. Report for the Southern Midlands Council, 15 pp.

Wray R.A.L. 1995 Solutional Landforms in Quartz Sandstones of the Sydney Basin. Unpublished PhD thesis. University of Wollongong, 381 pp.

Wray R.A.L. 1997a A global review of solutional weathering forms on quartz sandstones. *Earth Science Reviews,* 42(3): 137-160.

Wray R.A.L. 1997b Quartzite dissolution: karst or pseudokarst? *Cave and Karst Science,* 24(2): 81-86.

Wray. R.A.L. 2009 Phreatric drainage conduits within quartz sandstone: evidence from the Jurassic precipice sandstone, Carnarvon Range, Queensland, Australia. *Geomorphology,* 110(3-4): 203-211.

Wray, R.A.L. and Sauro, F. 2017 An updated global review of solutional weathering processes and forms in quartz sandstones and quartzites. *Earth Science Reviews,* 171: 520-557.

Young, R.W. 1987 Sandstone landforms of the tropical East Kimberley Region, Northwestern Australia. *The Journal of Geology,* 95(2): 205-218.

Helictite, (2019) 45**:** 39-50

A preliminary study of the use of hind limb skeletal elements to identify Australian rodent species (family Muridae) from Quaternary fossil cave deposits

Evan Parker
School of Biological Sciences, The University of Adelaide, Adelaide, South Australia, 5005.
evan.parker@adelaide.edu.au

Abstract

The hind limb bones from small mammals are some of the more abundant elements found within cave fossil deposits and may be useful for species identification where craniodental elements are lacking. In this paper the usefulness of the hind limb elements (tibiofibula and femur) for species-level identification of eight native Australian rodents (family Muridae) from six South Australian genera is studied. A qualitative and quantitative methodology was adopted and observed differences assessed in hind limb bone morphology. Differences are reported between species on each of the two hind limb elements allowing identification of bones to species level. Identification keys are constructed using the most common identifiable features of limb elements. Identification of the femur could be made using measurements, while the tibiofibula required both quantitative measures and qualitative observed differences. Measures were taken using only digital vernier callipers and support one of the aims of the study: to be able to identify the limb bones to species level in the field without any specialised equipment. Results support that the observed and measured morphological differences between hind limb elements can be used to accurately identify the eight studied Australian murid rodents to a species level.

Key words: *mammal, rodent, Muridae, postcranial elements, Quaternary, caves.*

Introduction

Mammal fossil bone assemblages are found in caves worldwide and provide insight into the environment, flora and fauna of the past (see Barnosky and others 2004, Fernandez-Jalvo 1996, Jass and George 2010, Price and others 2019). The bones within these deposits can represent time scales of hundreds to thousands of years and preserve evidence of the animals surrounding the location, predator interactions and environmental conditions. Palaeoecological data gained from small body-sized mammals offer finer resolution than larger mammals due to their smaller home range and high sensitivity to environmental change (López Antoñanzas and Cuenca Bescós 2002). This allows elucidation of changes in species range, relative abundance and ecosystem stability over time (Macken and Reed 2014, Brace and others 2012). Small mammal remains are prevalent in cave deposits, where accumulating agents such as predatory birds may concentrate deep deposits of bones (Andrews 1990). In particular, rodent species are often the most numerous in Quaternary cave deposits due to their high diversity, abundance in the community surrounding caves and susceptibility to predation by avian threats such as owls (Andrews 1990).

For many years small mammals from Quaternary deposits were disregarded by researchers in favour of their larger relatives (Andrews 1990). In the last 30 years smaller mammals have had something of a resurgence in palaeontological research. Key sites such as Gran Dolina in Spain (Campaña Lozano and others 2017, Fernandez-Jalvo 1995, 1996, Fernandez-Jalvo and Andrews 1992, López Antoñanzas and Cuenca Bescós 2002), areas of North-West Europe (Brace and others 2012) and in Australia the Mt. Etna and Naracoorte regions (Cramb and others 2018, Hocknull and others 2007, Macken and Reed 2013, 2014) have yielded data from small mammal assemblages to increase understanding of the palaeoenvironment over the middle to late Pleistocene.

Palaeoecological reconstructions are based on the diversity and abundance of species preserved within a fossil deposit as a proxy for the original faunal community. Determining the preferred habitat and ecological niche of these species allows inferences regarding the environment present at the time their bones were deposited into the assemblage. The correct identification of species within the deposit is of paramount importance when drawing accurate conclusions about past environments and faunal interactions.

Species identification is typically based on cranial elements (teeth, skulls and jaws) found within a fossil assemblage (Ungar 2010, Thies and others 2012). This is because these elements possess unique diagnostic characters that are preserved well in fossil specimens. Thies and others (2012) noted that both the maxilla and mandible are required for genus level identification in rodents and that recovering pairs of jaws from a single individual in fossil sites is rare. Consequently, the more numerous postcranial elements of rodents could offer an alternative for species identification when sorting through bulk fossil material or completing field investigations of an *in situ* assemblage.

The diagnostic characters of Australian rodent dentitions have been documented by several authors (Crowther 2002, McDowell and Medlin 2009, Watts and Aslin 1981). However, the morphological differences in limb elements have not been presented. Matisoo-Smith and Allen (2001) reported femoral length differences within distinct geographical populations of *Rattus exulans* throughout island habitats of the Pacific. Differences in femoral length of almost 10 mm were reported across locations with the authors concluding that the current method of identification is difficult in the pacific rat. Limb bones of tupaiids (Mammalia, Scandentia) have been shown to have significant morphological differences within a genus related to the substrate in which it lives (Sargis 2002a, 2002b, 2002c). Koper (2014) concluded that morphological differences in the forelimbs of *Canis dirus* and *C. lupus* can be used to identify species when there is an absence of dental material. Veatch and others (2019) used limb bone measurements to assess body size classes in rodent fossil assemblages from Liang Bua Cave in Indonesia as a means to assess palaeoenvironmental and habitat change during the late Pleistocene.

This paper presents a preliminary investigation of a method for identifying some Australian rodent species (family Muridae) based on hind limb proportions and the viability of this technique for use in palaeontological and archaeological investigations. The aim of the study was to determine if species level identifications can be made from disarticulated rodent hind limb elements which are abundant in Quaternary cave deposits, offering an alternative to teeth if the latter are poorly represented in the assemblage.

Methods and Materials

Comparative skeletal material from seven extant and one extinct Australian rodent species (family Muridae) were examined from the sub-fossil and mammal collections of the South Australian Museum and the ornithology and mammalogy sections of Museum Victoria. The study species were chosen based on their presence in many south-eastern Australian Quaternary cave sites such as the Naracoorte Caves in South Australia. The species studied and number of specimens are reported in Table 1. The average live body weight of the study species was determined based on values in Watts and Aslin (1981), Van Dyck and Strahan (2008) and Menkhorst (2004). Tools used for measurements were a set of calibrated digital vernier callipers (150 mm TradeQuip™ part number #4001) modified by removal of a 7 mm notch from the back of the secondary jaws in order to fit the measuring surface between the tibiofibula fusion point. Hind limbs were chosen for this study as they are robust, numerous and easily identifiable within a cave fossil deposit.

Table 1. Rodent species examined for this study and number of specimens (N) measured for each.

Species	N
Leporillus conditor	15
Hydromys chrysogaster	12
Mastacomys fuscus	8
Notomys mitchelllii	6
*Pseudomys gouldii**	12
Pseudomys shortridgei	12
Rattus fuscipes	8
Rattus lutreolus	7

* extinct species

Rodents have a specialised tibia and fibula complex, hereafter referred to as a tibiofibula. This complex fuses shortly after birth (Moss 1977) and is useful in distinguishing rodents from other small mammals within a bone assemblage in the absence of cranial elements. A total of 16 measures adapted from Sargis (2002c) were taken for the femur and the tibiofibula as shown in Figures 1A and 1B.

Two measurements for each limb element were taken and averaged to minimise measurement error (see Blackwell and others (2006)). Fourteen indices were calculated (nine femur and five tibiofibula, reported in Table 2) and measure different ratios between osteological features in a single bone. These indices also allow comparison between different sizes of rodent limb bones and account for differences among adults and juveniles of a species. Mid-point measures for the medio-lateral and antero-posterior diaphysis width were taken at the point marked by half of the total limb bone length. Observed qualitative features of each limb element such as rolling of the tibial crest and completeness of tibiofibula fusion were also recorded.

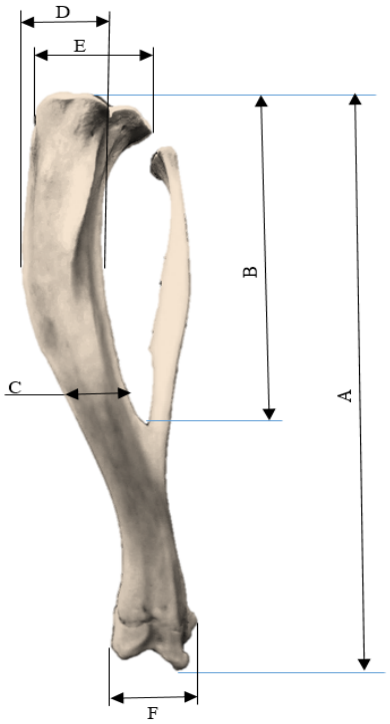

Figure 1A. Measurements taken from tibiofibula of Australian rodents (family Muridae);
A) total length, B) fusion point, C) Medio-lateral diaphysis width, D) diaphysis width at crest, E) proximal epicondyle width, F) distal epicondyle width. (Note. Antero-posterior diaphysis width was measured at the same point as medio-lateral diaphysis width as indicated in text.)

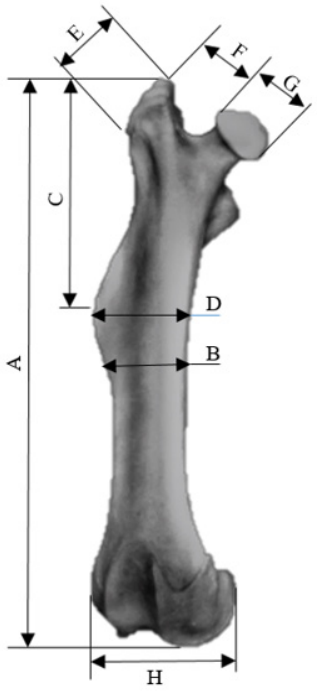

Figure 1B. Measurements taken from femur of Australian rodents (family Muridae) species in this study; A) total length, B) medio-lateral diaphysis width, C) third trochanter length, D) third trochanter width, E) length of greater trochanter, F) neck width, G) head width, H) distal epicondyle width. (Note. Antero-posterior diaphysis width was measured at the same point as medio-lateral diaphysis width as indicated in text.)

Table 2. Ratios and formulae calculated for limb bone measurements during this study

Description	Formula
Femoral diaphysis width index	(Femoral medio-lateral diaphysis width / Femoral total length) X 100
Femoral diaphysis thickness index	(Femoral antero-posterior diaphysis width / Femoral total length) X 100
Femoral third trochanter crest width index	(Femoral width of third trochanter crest / Femoral total length) X 100
Femoral third trochanter crest length index	(Femoral length of third trochanter / Femoral total length) X 100
Femoral third trochanter relative crest size index	([Femoral width of third trochanter - Femoral medio-lateral width] / Femoral total length) X 100
Femoral head length index	(Femoral largest head width / Femoral total length) X 100
Femoral head/neck ratio index	(Femoral largest head width / Femoral neck width) X 100
Femoral epicondyle/greater trochanter ratio index	(Femoral distal epicondyle width / Femoral length of greater trochanter) X 100
Femoral medio-lateral/epicondyle ratio index	(Femoral medio-lateral diaphysis width / Femoral distal epicondyle width) X 100
Tibiofibula diaphysis width index	(Tibiofibula medio-lateral diaphysis width / Tibiofibula total length) X 100
Tibiofibula diaphysis thickness index	(Tibiofibula antero-posterior width / Tibiofibula total length) X 100
Tibiofibula crest size index	(Tibiofibula diaphysis width at crest / Tibiofibula total length) X 100
Tibiofibula fusion point index	(Tibiofibula fusion point / Tibiofibula total length) X 100
Tibiofibula epicondyle ratio index	(Tibiofibula distal epicondyle width / Tibiofibula distal epicondyle width) X 100

Data were entered in SPSS™ for Windows. A one-way ANOVA was performed for the measured limb element data to report standard deviations and mean within each raw measure and computed ratio. A Post-Hoc Tukey HSD comparison for each limb bone and limb bone measure was executed to create species-based groups based on significant differences for each hind limb bone measure. The significance value was set at 0.05 ($p < 0.05$). Keys for each element were constructed using significant differences within each limb element. The most common differences were used to allow the simplest identification to species level. Specimen details are reported in Appendix 1.

Results

Overall limb length

An increase in mean length of the femur and tibiofibula is generally consistent with an increase in the total average animal live weight (Figure 2A and Table 3). A notable exception is the tibiofibula and femur of *Notomys mitchellii* indicated at point 'A' in Figure 2A. Despite being one of the smaller species by live weight (avg. 52 grams), *N. mitchellii* has the third longest mean tibiofibula length at 36.5 mm. Figure 2B shows an image of the difference in size from *N. mitchellii* to *H. chrysogaster*.

The femur of *N. mitchellii* is longer than expected if a linear relationship existed between femur length and live animal weight. Notomys *mitchellii* has a live weight approximately the same as *Pseudomys gouldii* (52 g and 50 g respectively); however, the femur length of 25.8 mm is similar to that of heavier species *Rattus fuscipes* (27.1 mm, mean weight 125 g, $p = 0.991$), *Rattus lutreolus* (28.2 mm, 122 g, $p = 0.724$), *Mastacomys fuscus* at (30.1 mm, 122 g, $p = 0.084$) and slightly longer than *P. shortridgei* (24.79 mm, 70 g, $p = 0.996$). The other species of a similar live weight, *P. gouldii*, had a mean femur length of 18.6 mm, significantly shorter than *N. mitchellii* ($p < 0.001$).

Tibiofibula quantitative index measure

Measurements of the tibiofibula between species showed differences in diaphysis width index, diaphysis thickness index, tibiofibula crest size index and tibiofibula fusion point index (Table 3).

Diaphysis width index for *N. mitchellii* was significantly smaller (4.6) than all other species examined with *P. gouldii* (5.2, $p = 0.031$) and *M. fuscus* (5.3, $p = 0.003$) closest on the post-hoc Tukey HSD. The tibiofibula diaphysis thickness index was not significantly different from other species. The tibiofibula of *H. chrysogaster* shows a significantly higher diaphysis thickness index (9.0) than its closest comparator, *Leporillus conditor* (6.4, $p < 0.001$), but the diaphysis width index (6.5) is not significantly different from that of other large species (*L. conditor*, $p = 0.926$, *R. lutreolus*, $p = 0.103$). No other species showed significant differences in the diaphysis thickness index or diaphysis width index. Tibiofibula crest size index showed only one identifiable species, *H. chrysogaster*, with a significantly larger crest index at 12.1 ($p < 0.001$) than other species. No other species is directly identifiable. The tibiofibula fusion point for *N. mitchellii* was significantly closer to the proximal end of the tibiofibula than any other species at an index point of 44.6. The other seven species ranged from 49.9 (*M. fuscus, p* < 0.001) to 55.8 (*H. chrysogaster, p* < 0.001). *Rattus fuscipes* had a significantly different tibiofibula fusion point index from *R lutreolus* (51.1 and 55.8 respectively, $p < 0.001$).

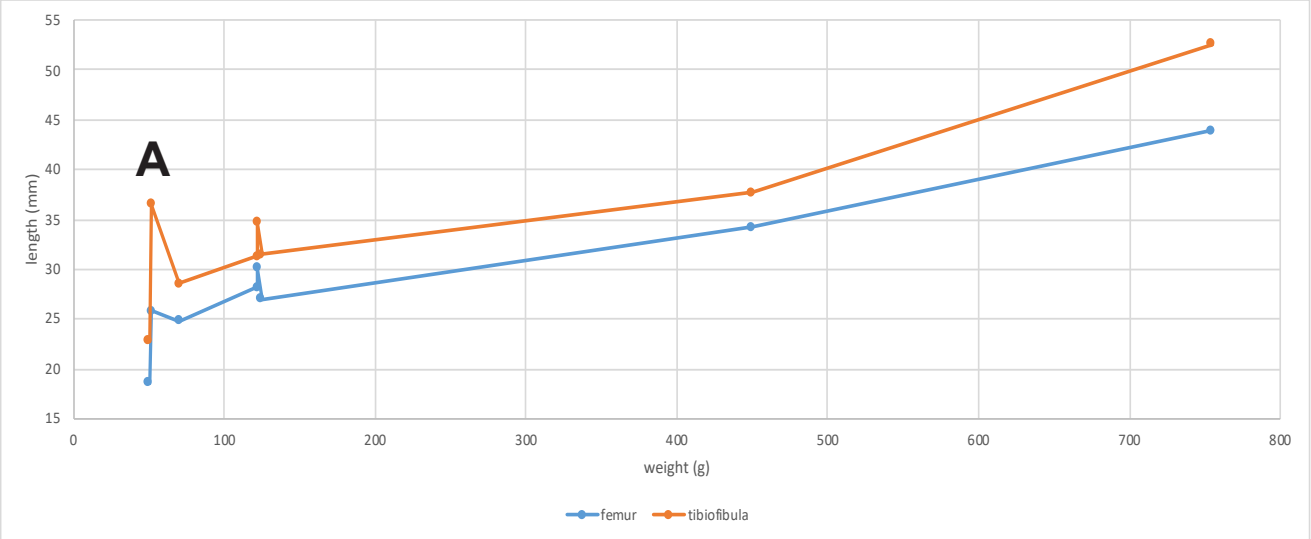

Figure 2A. Average live weight vs. average hind limb length of measured Australian murid rodents selected in this study. Sizes for species are reported in Table 3.

Figure 2B. Tibiofibulae and femora of selected species present in this study. From left to right: *N. mitchellii, P. shortridgei* (femur only), *R. lutreolus, R. fuscipes, L. conditor, H. chrysogaster.* Scale bar = 10 mm.

Tibiofibula qualitative measures

Three qualitative differences were also observed in the tibiofibula. *Hydromys chrysogaster* showed a flattening of the proximal side of the mediolateral face of the tibial crest. This flattening occurred between the proximal epiphysis and the tibiofibula mid-point and is represented in Figure 3A. *Mastacomys fuscus* showed a pronounced 'rolling' of the tibial crest (Figure 3B). This 'rolling' occurred on the posterior of the proximal end of the tibial crest and curved from the lateral towards the medial side of the bone. *Leporillus conditor* showed an observable difference in the fusion of the tibia and fibula (Figure 3C). The fusion point index is not significantly different from other species at 54.4 (e.g. *H. chrysogaster,* $p = 0.935$) but there is a separation of the fusion of the two bones towards the distal end. No other species showed this trait and all had more complete fusion.

Femur quantitative index measures

Femur diaphysis width index showed identifiable differences in two species at the lower and upper end of the results. *Notomys mitchellii* showed the smallest value at 7.3, significantly smaller than all other species including *P. gouldii* (9.7, $p < 0.001$) which is similar in live weight. *Hydromys chrysogaster* was significantly larger than all other species with a result almost twice as large as *N. mitchellii* at 14.4 and significantly larger than *L. conditor* (11.6, $p < 0.001$). Diaphysis thickness index showed no species with significant differences from all other species. *Leporillus conditor* (9.2) and *H. chrysogaster* (9.4) were significantly larger than all other species observed, although the difference between these species was not significant ($p = 0.929$). Third trochanter crest width index allowed two species to be identified. *N. mitchellii* was significantly smaller than all other species at 11.6 ($p < 0.001$) and *H. chrysogaster* was significantly larger than all other species at 17.1 ($p < 0.001$). All other species showed no significant differences among them. Third trochanter crest length index showed two species were significantly different: *Leporillus conditor* (38.2, $p = 0.002$) and *Hydromys chrysogaster* (45.7, $p < 0.001$).

Femur head/neck index showed that only one species, *L. conditor,* was significantly different from all other species at an index of 177.8, *R. lutreolus* was the closest with an index of 153.1 but remained significantly different ($p = 0.020$). Femur mediolateral diaphysis/epicondyle width index showed that only *N. mitchellii* had a significantly different measurement index from all other species at 47.9 ($p < 0.001$).

Table 3. Average computed hind limb ratios and measurements from eight Australian rodent species (family Muridae).

		FEMUR									
Species	live weight (g)	Femur total length (mm)	Diaphysis width index	Diaphysis thickness index	Third trochanter crest width index	Third trochanter crest length index	Relative third trochanter size index	Femur Head Length index	Femur Head Neck Index	Femur epicondyle/ greater trochanter index	Femur mediolateral/ epicondyle index
H. chrysogaster	755	43.9	14.4*	9.4	17.1*	45.7*	2.7	12.0	127.4	195.1	56.6
L. conditor	450	34.2	11.6	9.2	14.8	38.2*	3.2	11.4	177.8*	149.1	57.3
R. fuscipes	125	27.1	10.7	8.3	14.4	34.9	3.7	9.7	140.1	179.7	60.9
M. fuscus	122	30.1	10.3	7.7	14.7	35.1	4.4	10.0	152.9	169.5	57.5
R. lutreolus	122	28.2	10.1	8.2	14.5	35.4	4.4	10.0	153.1	169.8	54.2
P. shortridgei	70	24.8	9.1	7.4	13.3	32.7	4.2	9.2	151.8	148.0	55.6
N. mitchellii	52	25.8	7.3*	7.0	11.6*	28.6	4.2	8.5	128.3	136.3	47.9*

		TIBIOFIBULA					
Species	live weight (g)	Tibiofibula total length (mm)	Tibiofibula diaphysis width index	Tibiofibula diaphysis thickness index	Tibiofibula crest size index	Tibiofibula fusion point index	Tibiofibula epicondyle index
H. chrysogaster	755	52.6	6.5	9.0*	12.1*	53.5	79.7
L. conditor	450	37.7	6.3	6.4	9.7	54.4	67.7
R. fuscipes	125	31.5	5.7	5.8	8.3	51.1	81.6
M. fuscus	122	34.7	5.3	5.9	6.4	49.9	72.9
R. lutreolus	122	31.3	6.1	6.1	9.1	55.8	75.2
P. shortridgei	70	28.6	5.4	6.0	8.4	52.1	85.6
N. mitchellii	52	36.5	4.6*	6.0	7.2	44.6*	77.8
P. gouldii	50	22.8	5.2	5.5	7.7	55.5	63.9

* significant difference $p < 0.05$

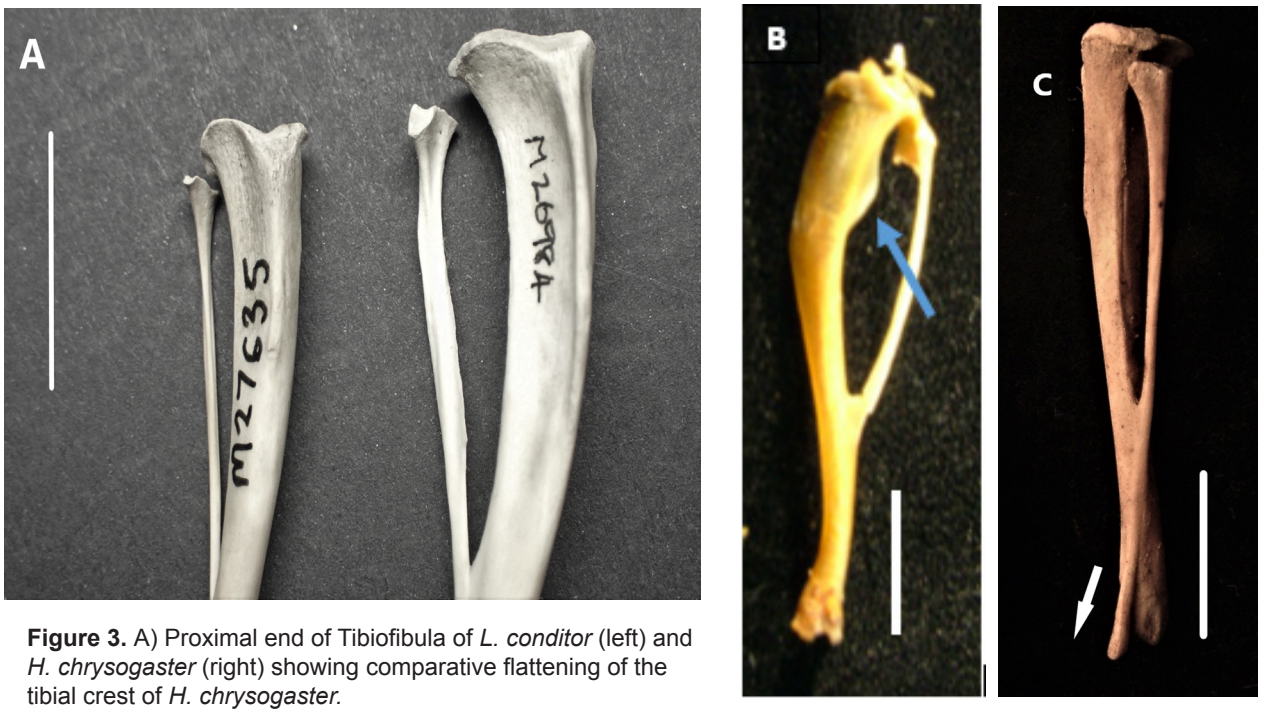

Figure 3. A) Proximal end of Tibiofibula of *L. conditor* (left) and *H. chrysogaster* (right) showing comparative flattening of the tibial crest of *H. chrysogaster.*

B) Tibiofibula of *M. fuscus* showing rolling of the tibial crest (indicated by arrow),

C) Tibiofibula from *Leporillus conditor* showing the 'Fusion Separation' described in the text (indicated by arrow). Scale bar = 10 mm.

Identification keys

The tibiofibula key is shown in Figure 4. In this key qualitative osteological features of separation in tibiofibula fusion (see Figure 3C) and rolling of the tibial crest (Figure 3B) identify *L. conditor* and *M. fuscus* respectively. Total tibiofibula length differentiates *H. chrysogaster* (< 45.5 mm), *P. shortridgei* (24.5 to 30 mm) and *P. gouldii* (< 24.5 mm). The tibiofibula fusion point is able to identify the remaining three species. *N. mitchellii* has a fusion point less than 47, *R. fuscipes* has a fusion point between 47 and 53.5 and *R. lutreolus* has a fusion point greater than 53.5. These values are based greater than one standard deviation from the mean of total length and tibiofibula fusion point to eliminate error through crossover of standard deviations.

The femur identification key is shown in Figure 5. Total femur length was able to identify *P. gouldii* with a length less than 21 mm. The remaining seven species were then divided into the larger species above 30 mm, *H. chrysogaster* (mean = 43.9 mm), *L. conditor* (mean = 34.3 mm) and *M. fuscus* (mean = 30.1 mm), and other species *R. fuscipes* (mean = 27.1 mm), *R. lutreolus* (mean = 28.2 mm), *P. shortridgei* (mean = 24.8 mm) and *N. mitchellii* (mean = 25.8 mm). *Hydromys chrysogaster* has a femur length above 30 mm with a diaphysis width index greater than 13.3, both *L. conditor* and *M. fuscus* have a total length above 30 mm and a diaphysis width index smaller than 13.3. Third trochanter crest length index was able to separate *L. conditor* (above 36.5) and *M. fuscus* (below 36.5). In species with a total femur length between 21 mm and 30 mm, diaphysis width index was able to identify *N. mitchellii* (< 8.2) from *P. shortridgei*, *R. fuscipes* and *R. lutreolus*. *Pseudomys shortridgei* has a third trochanter crest width index less than 13.8 while *R. lutreolus* and *R. fuscipes* have a value above 13.8. *Rattus lutreolus* and *R. fuscipes* showed a significant difference ($p = 0.007$) on medio-lateral epicondyle index with *R. lutreolus* less than 57.5 and *R. fuscipes* greater than 57.5.

Discussion

The increase in total length of hind limbs (femur and tibiofibula) in relation to the average live weight of the species studied here represented an almost linear relationship for all species except *N. mitchellii* (Figure 2A). *N. mitchellii* had a longer tibiofibula and femur than its relatively low live weight (52 g) would suggest. The longer length of the tibiofibula also altered the tibiofibula diaphysis width index and gave a physical appearance of a more gracile and less robust tibiofibula than other species, as seen in Figure 2B. The elongated nature of the tibiofibula and the femur (to a lesser extent) of *N. mitchellii* are likely related to the form of locomotion that give rise to the common name for the various species of *Notomys*, the 'hopping mice'. The difference in tibiofibula and femoral length of *N. mitchellii* and *P. gouldii* (species of a similar weight), suggests that *P. gouldii* can be assigned an accurate identification based on having a significantly smaller total length of both elements (tibiofibula < 24.5 mm, femur < 21 mm). The total length of the hind limb elements of *H. chrysogaster* is of sufficient size to identify the tibiofibula with a length over 45.5 mm; however, the femur length above 30 mm needed to be combined with a diaphysis width above 13.3 to ensure accurate identification.

Quantitatively, the total tibiofibula length could be used to identify three species in the absence of any qualitative measures (rolling of the tibial crest and incomplete fusion of the tibia and fibula) as noted in the text. *Hydromys chysogaster* had a tibiofibula length over 45.5 mm, *P. shortridgei* had a length between 24.5 mm and 30 mm and *P. gouldii*, the smallest studied species at 50 g live weight, was identifiable if the value for the tibiofibula total length was less than 24.5 mm. Diaphysis thickness index was a useful measure for confirming the difference between *H. chrysogaster* and other species although was not included in the identification key. Instead, total length was included as this measure does not require any calculations. The tibiofibula fusion point was significantly different for only *N. mitchellii* compared to all other species; however, there was a significant difference between *R. lutreolus* and *R. fuscipes*. This was the only differentiating factor between the *Rattus* species and is included as an identifying measure within the key.

Qualitative identifying features on the tibiofibula included rolling of the tibial crest in *M. fuscus*, flattening of the tibial crest in *H. chrysogaster* and distal separation of fusion in *L. conditor*. These observations were pronounced enough to identify species based on their presence but only two are recorded in the key. The flattening of the tibial crest in *H. chrysogaster* was not included in the identification key as the total length of the bones was a more measurable difference between the eight species, as shown in Figure 2B. The separation of fusion present in the distal tibiofibula of *L. conditor* was observed in all specimens, this was rarely the case for other species. The rolling of the tibial crest was useful in identifying *M. fuscus* from other species with similar tibiofibula total lengths such as *R. fuscipes* or *R. lutreolus* and was included in the key as the identifying characteristic for *M. fuscus* tibiofibula.

Figure 4.
Key for identification of rodent tibiofibula elements measured in this study using a combination of total measurements (as indicated by millimetres after number), indices (values) and qualitative observations (yes/no).

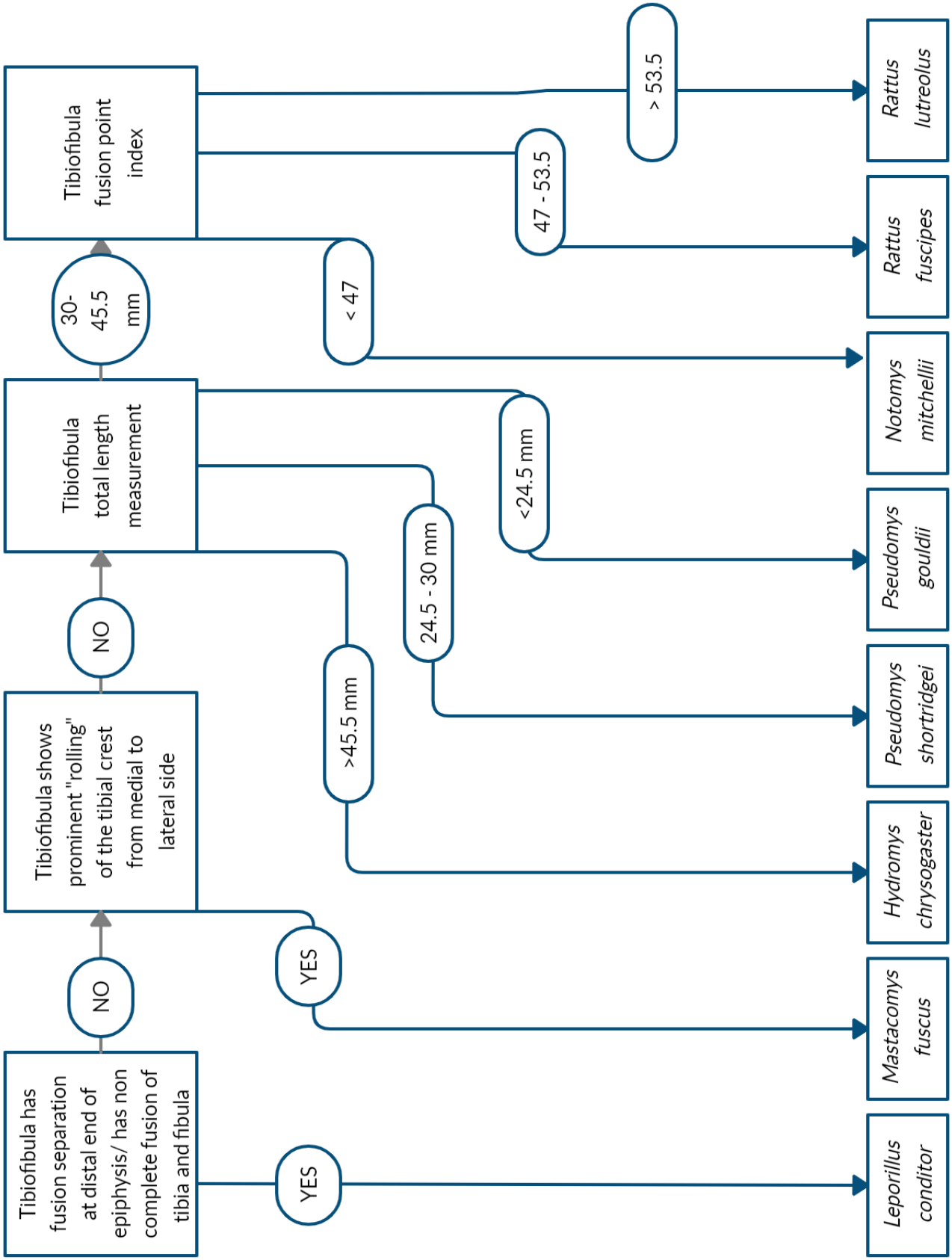

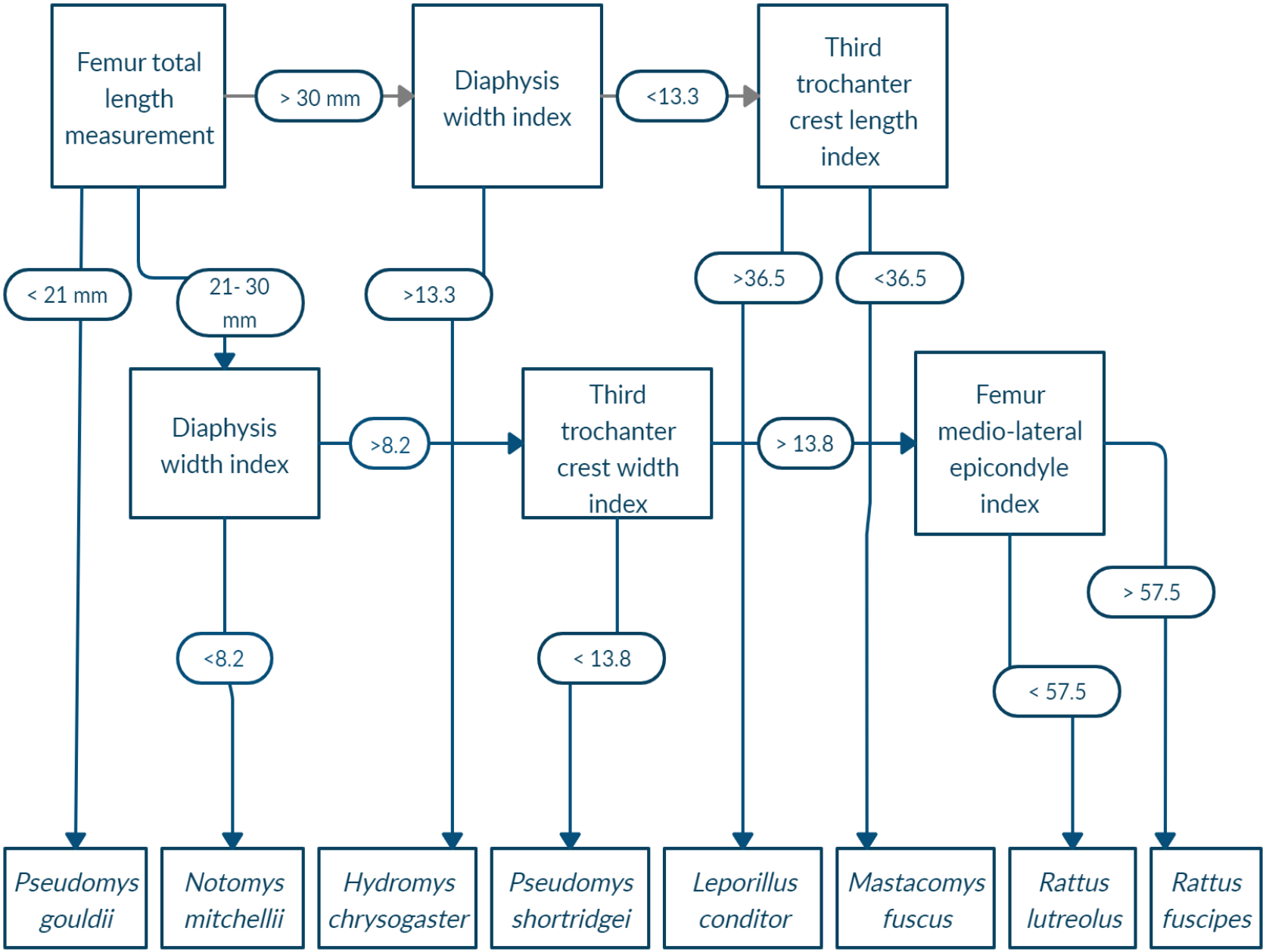

Figure 5.
Key for identification of rodent femur elements measured in this study using a combination of total measurements (as indicated by millimetres after number) and indices (values).

Femoral qualitative measures were not observed. Identification of the femur to species level is based on the measured indices and total limb length. *Pseudomys gouldii* had the smallest total length of femur, significantly different from all other species (18.59, $p < 0.001$) and this was used as the first identifiable species measure. Femora with a longer total length than *P. gouldii* were then grouped into those species above 30 mm (*H. chrysogaster*, *L. conditor* and *M. fuscus*) and those between 21 mm and 30 mm (*N. mitchelli, P. shortridgei, R. fuscipes* and *R. lutreolus*). In the group of smaller total length of femur, *N. mitchellii* had a significantly smaller diaphysis width index (<8.2, $p < 0.001$) compared to all other species in the group and therefore this measure was used for positive identification. The third trochanter crest width index allowed identification of *P. shortridgei* if it was below 13.8 and the diaphysis width index was greater than 8.2. The two *Rattus* species had a third trochanter crest width index above 13.8 and a diaphysis width index above 8.2. The femur medio-lateral epicondyle index showed a significant difference between *R. lutreolus* and *R. fuscipes* ($p = 0.007$). *Rattus lutreolus* had a femur medio-lateral diaphysis width index below 57.5 and *R. fuscipes* had a value above 57.5. A femur total length above 30 mm and a diaphysis width index greater than 13.3 identified *H. chrysogaster*. Third trochanter crest length index was able to identify *M. fuscus* (values less than 36.5) and *L. conditor* (values above 36.5) when combined with a total femur length of above 30 mm and a diaphysis width index of less than 13.3.

The keys provided in this paper offer a means of identification for the rodent hind limbs that are present within fossil bone assemblages and are primarily to be used on single, disarticulated elements. The femoral identification is based solely on the quantitative measurements and computed indices, whereas the tibiofibula, an unusual complex with fused limb elements, combined with observed qualitative features, enables one to differentiate two of the eight species.

This study is limited by the small species diversity for each of the six Australian rodent genera chosen, that is four genera have only a single species in them (*Hydromys, Mastacomys, Leporillus* and *Notomys*) and further investigation into the differences within a single genus may yield useful identification measures. More replications of chosen species from different geographical regions may add greater certainty to the results.

Conclusion

This research aimed to investigate morphological differences within Australian rodent hind limbs (family Muridae) in order that researchers and interested parties (e.g. cavers) could make field-based decisions on the rodent fossils found within many cave sites. Results indicate that osteological differences observed are not linked in a linear relationship to the live weight of the animal. Significant differences were observed between all species studied allowing identification of each of the hind limb elements to species level. Rodents that exhibit habitual differences such as hopping (*N. mitchelli*) or swimming (*H. chrysogaster*) showed the greatest number of significant differences in hind limb proportions from all other species. Femoral identification was based solely on quantitative measures and indices; whereas tibiofibula identification was based on a mix of quantitative and qualitative measures. The preliminary results from this study appear to support the combination of total measurements, computed indices and morphological difference for species level identification of Australian murid rodent hind limb elements in Quaternary fossil deposits.

Acknowledgements

This research was completed in part as an Honours project undertaken at the Flinders University of South Australia. EP would like to acknowledge David Stemmer and Graham Medlin from the South Australian Museum for access to comparative samples and advice during my research, Rory O'Brien for the loan of rodent skeletal material from the Victorian Museum's collection and the guidance and support of my supervisors Dr Liz Reed and Dr Ken Sanderson. Thanks are also given to the editor and reviewers whose suggestions have greatly improved this manuscript. This research has no financial support to acknowledge.

References

Andrews, P. 1990 *Owls, Caves and Fossils* Chicago, U.S.A., University of Chicago Press.

Barnosky, A.D., Bell, C.J., Emslie, S.D., Goodwin, T.H., Mead, J.I., Repenning, C.A., Scott, E. & Shabel, A.B. 2004 Exceptional record of mid-Pleistocene vertebrates helps differentiate climatic from anthropogenic ecosystem perturbations. *Proceedings of the National Academy of Sciences of the United States of America*, 101(25): 9297-9302. https://doi.org/10.1073/pnas.0402592101

Blackwell, G.L., Bassett, S.M. & Dickman, C.R. 2006 Measurement error associated with external measurements commonly used in small-mammal studies. *Journal of Mammalogy,* 87: 216-223.

Brace, S., Palkopoulou, E., Dalen, L., Lister, A.M., Miller, R., Otte, M., Germonpre, M., Blockley, S.P.E., Stewart, J.R. & Barnes, I. 2012 Serial population extinctions in a small mammal indicate Late Pleistocene ecosystem instability. *Proceedings of the National Academy of Sciences of the United States,* 109: 20532-20536.

Campaña Lozano, I., Benito Calvo, A., Pérez-González, A., Ortega, A., Bermúdez De Castro, J.-M. & Carbonell, E. 2017 Pleistocene sedimentary facies of the Gran Dolina archaeo-paleoanthropological site (Sierra de Atapuerca, Burgos, Spain). *Quaternary International,* 433: 68-84.

Cramb, J., Price, G.J. & Hocknull, S.A. 2018 Short-tailed mice with a long fossil record: the genus Leggadina (Rodentia: Muridae) from the Quaternary of Queensland, Australia. *PeerJ,* 6, e5639 https://doi.org/10.7717/peerj.5639

Crowther, M.S. 2002 Morphological variation within *Antechinus agilis* and *Antechinus stuartii* (Marsupialia : Dasyuridae). *Australian Journal of Zoology,* 50: 339-356.

Fernandez-Jalvo, Y. 1995 Small mammal taphonomy at La Trinchera de Atapuerca (Burgos, Spain). A remarkable example of taphonomic criteria used for stratigraphic correlations and palaeoenvironment interpretations. *Palaeogeography, Palaeoclimatology, Palaeoecology,* 114: 167-195.

Fernandez-Jalvo, Y. 1996 Small mammal taphonomy and the middle Pleistocene environments of Dolina, northern Spain. *Quaternary International,* 33: 21-34.

Fernandez-Jalvo, Y. & Andrews, P. 1992 Small mammal taphonomy of Gran Dolina, Atapuerca (Burgos), Spain. *Journal of Archaeological Science,* 19: 407-428.

Hocknull, S.A., Zhao, J.-X., Feng, Y.-X. & Webb, G.E. 2007 Responses of Quaternary rainforest vertebrates to climate change in Australia. *Earth and Planetary Science Letters,* 264: 317-331.

Jass, C.N. & George, C.O. 2010 An assessment of the contribution of fossil cave deposits to the Quaternary paleontological record. *Quaternary International,* 217: 105-116.

Koper, L. 2014 The devil is in the details: identification of postcranial elements of *Canis dirus* and *Canis lupus* from Rancho La Brea using discriminant function and morphometric analyses. *Faseb Journal,* 28(1) supp.

López Antoñanzas, R. & Cuenca Bescós, G. 2002 The Gran Dolina site (Lower to Middle Pleistocene, Atapuerca, Burgos, Spain): new palaeoenvironmental data based on the distribution of small mammals. *Palaeogeography, Palaeoclimatology, Palaeoecology,* 186: 311-334.

Macken, A. & Reed, E. 2013 Late Quaternary small mammal faunas of the Naracoorte Caves World Heritage Area. *Transactions of the Royal Society of South Australia,* 137: 53-67.

Macken, A. & Reed, E.H. 2014 Postglacial reorganization of a small-mammal paleocommunity in southern Australia reveals thresholds of change. *Ecological Monographs,* 84: 563-577.

Matisoo-Smith, E. & Allen, J. 2001 Name that rat: Molecular and morphological identification of Pacific rodent remains. *International Journal of Osteoarchaeology,* 11: 34-42.

McDowell, M. & Medlin, G. 2009 Mammal remains, including the White-footed Rabbit-rat *'Conilurus albipes'*, from the Fleurieu Peninsula, South Australia. *The South Australian Naturalist,* 83: 26-28.

Moss, M.L. 1977 A functional analysis of fusion of the tibia and fibula in the rat and mouse. *Cells Tissues Organs,* 97: 321-332.

Price, G.J., Louys, J., Smith, G.K. & Cramb, J. 2019 Shifting faunal baselines through the Quaternary revealed by cave fossils of eastern Australia. *PeerJ,* 6, e6099.

Sargis, E.J. 2002a Functional morphology of the forelimb of tupaiids (Mammalia, Scandentia) and its phylogenetic implications. *Journal of Morphology,* 253: 10-42.

Sargis, E.J. 2002b Functional morphology of the hindlimb of tupaiids (Mammalia, Scandentia) and its phylogenetic implications. *Journal of Morphology,* 254: 149-185.

Sargis, E.J. 2002c A multivariate analysis of the postcranium of tree shrews (Scandentia, Tupaiidae) and its taxonomic implications. *Mammalia,* 66: 579-598.

THIES, M., TUTALO, R., LABBE, M.D. & LEWIS, P. 2012 Assessing the difficulties of genus-level diagnoses of fossil rodents (Conference Poster and Abstract). *Journal of Vertebrate Paleontology,* 32: 183-183.

UNGAR, P.S.A. 2010 *Mammal teeth: origin, evolution, and diversity*. Johns Hopkins University Press, Baltimore, MD.

VEATCH, E.G., TOCHERI, M.W., SUTIKNA, T., MCGRATH, K., WAHYU SAPTOMO, E., JATMIKO & HELGEN, K.M. 2019 Temporal shifts in the distribution of murine rodent body size classes at Liang Bua (Flores, Indonesia) reveal new insights into the paleoecology of *Homo floresiensis* and associated fauna (Report). *Journal of Human Evolution,* 130: 45-60.

WATTS, C.H.S. & ASLIN, H.J. 1981 *Rodents of Australia.* Angus & Robertson, Sydney.

Appendix 1. Specimen registration details for eight Australian murid rodents examined for this study

Leporillus conditor	M21372	M21396	83SF6-1	83SF6-2	83SF6-7	83SF6-8
	83SF6-3	83SF6-4	83SF6-5	83SF6-6	83SF6-9	83SF6-10
	83SF6-11					
Hydromys chrysogaster	M22268	M8287	M3533	M1639	C29746	C29798
	M1638	M1637	M20174	M17788	C20283	C29684
Mastacomys fuscus	C11656	C25989	C11508	C25086	C15026	C22529
	C15674	C15033				
Notomys mitchellii	C15021	C2866	C11357	C10301	C16236	C11333
Pseudomys shortridgei	C21598	C19923	C22111	C21599	C9648	C16049
	C22125	C16050	C19925	C27069	C22113	C22134
Pseudomys gouldii	CHG.11.12.1.p	CHG.11.13.1.p	CHG.11.15.1.p	CHG.11.17.1.p	ARD.1.33.1.p	ARD.1.215.1p
	CHG.11.24.1.p	ARD.1.3.1.p	ARD.1.9.1.p	ARD.1.40.1.p	ARD.1.215.2p	CHG.3.21.1.p
Rattus lutreolus	C12748	C26004	C25794	C8701	C10164	C20129
	C26622	C10163				
Rattus fuscipes	M10399	M19815	M10398	M10396	M10401	M10397
	M10400					

HELICTITE

END OF VOLUME 45